THE JOURNAL OF BIOLOGICAL CHEMISTRY VOL. 282, NO. 52, pp. 37325–37340, December 28, 2007

Characterization of a Globin-coupled Oxygen Sensor with a Gene-regulating Function*[S]

Received for publication, July 6, 2007, and in revised form, September 27, 2007 Published, JBC Papers in Press, October 9, 2007, DOI 10.1074/jbc.M705541200

Liesbet Thijs[‡], Evi Vinck[§1], Alessandro Bolli[¶], Florin Trandafir[§], Xuehua Wan[‖], David Hoogewijs[**], Massimiliano Coletta[‡‡], Angela Fago[§§], Roy E. Weber[§§], Sabine Van Doorslaer[§], Paolo Ascenzi[¶¶], Maqsudul Alam[‖], Luc Moens[‡], and Sylvia Dewilde[‡2]

From the Departments of [‡]Biomedical Sciences and [§]Physics, University of Antwerp, Universiteitsplein 1, B-2610 Antwerp, Belgium, the [¶]Dipartimento di Biologia and Laboratorio Interdipartimentale di Microscopia Elettronica, Università Roma Tre, Viale G. Marconi 446, 00146 Roma, Italy, the [‖]Department of Microbiology, University of Hawaii, Honolulu, Hawaii 96822, the [**]Department of Biology and Centre for Molecular Phylogeny and Evolution, Ghent University, K .L. Ledeganckstraat 35, 9000 Ghent, Belgium, the [‡‡]Dipartimento di Medicina Sperimentale e Scienze Biochimiche, Università di Roma Tor Vergata, Via Montpellier 1, 00133 Roma, Italy, [§§]Zoophysiology, Department of Biological Sciences, University of Aarhus, DK-8000 Aarhus C, Denmark, and [¶¶]Istituto Nazionale per le Malattie Infettive Lazzaro Spallanzani, Via Portuense 292, 00149 Roma, Italy

Globin-coupled sensors (GCSs) are multiple-domain transducers, consisting of a regulatory globin-like heme-binding domain and a linked transducer domain(s). GCSs have been described in both Archaea and bacteria. They are generally assumed to bind O_2 (and perhaps other gaseous ligands) and to transmit a conformational change signal through the transducer domain in response to fluctuating O_2 levels. In this study, the heme-binding domain, *Av*GReg178, and the full protein, *Av*GReg of the *Azotobacter vinelandii* GCS, were cloned, expressed, and purified. After purification, the heme iron of *Av*GReg178 was found to bind O_2. This form was stable over many hours. In contrast, the predominant presence of a bis-histidine coordinate heme in ferric *Av*GReg was revealed. Differences in the heme pocket structure were also observed for the deoxygenated ferrous state of these proteins. The spectra showed that the deoxygenated ferrous derivatives of *Av*GReg178 and *Av*GReg are characterized by a penta-coordinate and hexa-coordinate heme iron, respectively. O_2 binding isotherms indicate that *Av*GReg178 and *Av*GReg show a high affinity for O_2 with P_{50} values at 20 °C of 0.04 and 0.15 torr, respectively. Kinetics of CO binding indicate that *Av*GReg178 carbonylation conforms to a monophasic process, comparable with that of myoglobin, whereas *Av*GReg carbonylation conforms to a three-phasic reaction, as observed for several proteins with bis-histidine heme iron coordination. Besides sensing ligands, *in vitro* data suggest that *Av*GReg(178) may have a role in O_2-mediated NO-detoxification, yielding met*Av*GReg(178) and nitrate.

Microorganisms often have at their disposal sensors that enable them to detect fluctuations in O_2, CO, and NO levels and induce signal cascades as specific adaptive responses. Key regulators in this mechanism are the "heme-based sensors" (1–7). Some well known examples of this class are the FixLJ system (8), EcDos (9), AxPDEA1 (10), CooA (11), and the HemATs (12). A common feature of FixL, EcDos, and AxPDEA1 is the N-terminal heme-binding PAS (Per-ARNT-Sim) domain. In brief, the PAS folding consists of a set of α-helices (Cα, Dα, Eα, and Fα) and a network of five antiparallel β-strands (Aβ, Bβ, Gβ, Hβ, and Iβ) with the heme-linked proximal histidine (Fα 3 histidine) as the most conserved residue. PAS domains are characterized by a predominantly hydrophobic heme distal pocket (7). FixL, EcDos, and AxPDEA1 specifically sense changes in environmental O_2 levels even though the response differs as a consequence of the different linked enzymatic domain(s). In FixL, a drop in O_2 tension leads to activation of the kinase domain that catalyzes a phosphoryl transfer from ATP to FixJ. FixJ-P acts as a transcription factor that induces gene expression involved in nitrogen fixation (13). The signaling domains of AxPDEA1 and EcDos are very similar. This region includes two domains, the GGDEF (domain with the Gly-Gly-Asp-Glu-Phe motif) and the EAL domain (domain with a conserved Glu-Ala-Leu motif) (14). The GGDEF domain catalyzes the formation of c-di-GMP[3] from two molecules of GTP, whereas the EAL domain has phosphodiesterase activity and hydrolyzes c-di-GMP. In AxPDEA1, phosphodiesterase activity is observed under hypoxic conditions. Because of the degradation of c-di-GMP, which is an

* This work was supported by the Fund for Scientific Research of Flanders, the Danish Natural Science Research Council, the Novo Nordisk Foundation, and National Science Foundation Grant MCB0446431. The costs of publication of this article were defrayed in part by the payment of page charges. This article must therefore be hereby marked "*advertisement*" in accordance with 18 U.S.C. Section 1734 solely to indicate this fact.

[S] The on-line version of this article (available at http://www.jbc.org) contains supplemental text, Tables S1–S2 and Figs. S1–S5.

[1] Research assistant of the Fund for Scientific Research of Flanders.

[2] Postdoctoral fellow of the Fund of Scientific Research Flanders. To whom correspondence should be addressed: Dept. of Biomedical Sciences, University of Antwerp, Campus Drie Eiken, Universiteitsplein 1, B-2610 Antwerp, Belgium. Tel.: 32-3-8202392; Fax: 32-3-8202339; E-mail: sylvia.dewilde@ua.ac.be.

[3] The abbreviations used are: c-di-GMP, cyclic diguanosine monophosphate; GCS(s), globin-coupled sensor(s); HS, high spin; LS, low spin; Mb, myoglobin; Ngb, neuroglobin; RR, resonance Raman; SVD, singular value decomposition; *Av*GReg, *A. vinelandii* Greg; *Av*GReg$^+$, open fast form of the full molecule *Av*GReg; *Av*GReg$^\#$, closed slow form of the full molecule *Av*GReg; *Av*GReg178$^+$, open fast form of the heme-binding domain of *Av*GReg; *Av*GReg178$^\#$, closed slow form of the heme binding domain of *Av*GReg; flavoHb, flavohemoglobin; trHb, truncated hemoglobin; legHb, leghemoglobin; DTT, dithiothreitol; Tricine, *N*-[2-hydroxy-1,1-bis(hydroxymethyl)ethyl]glycine; CW, continuous wave.

allosteric activator of cellulose synthase (15, 16), cellulose is not produced. Recently, EcDos has also been found to function as a c-di-GMP-specific phosphodiesterase (9). A special heme-binding protein is CooA with its *b*-type heme. CooA is a CO-sensing transcription factor that governs the oxidation of CO to CO_2 (11).

The most recently discovered subclasses of heme-based sensors in prokaryotes are the "globin-coupled sensors" (GCS), with the HemATs as the best studied. As suggested by the name "GCS," the sensor domain has a typical α-helical globin fold. Hou and co-workers (12) first reported that the sensor domain of the HemATs of *Bacillus subtilis* and *Halobacterium salinarium* shows myoglobin (Mb)-like absorption spectra and selectively binds O_2. This selectivity is probably related to specific H-bonding between O_2 and key amino acid residues (17, 18). The second domain consists of a methyl-accepting domain, which triggers the aerotactic response. In general, however, other functions are also hypothesized for the signaling domains of GCS. These domains may be involved in gene-regulating functions, in protein-protein interactions, or in yet unknown functions (19).

In this study, we report the characterization of the GCS of *Azotobacter vinelandii* (*Av*GReg). *A. vinelandii* is a free-living aerobic N_2-fixing bacterium commonly found in soil, where CO and NO are typically found in trace amounts (20). Soil is the most important biological sink for CO in nature. Although there is no evidence for metabolizing CO as a carbon source in *A. vinelandii*, Youn and co-workers (21) identified CooA homologues by searching the data base of diverse microorganisms. Additionally, NO is a naturally occurring soil component that is produced and consumed by diverse microorganisms. NO, which can diffuse out of the cell, is an intermediate of the denitrification cycle, converting nitrogen to dinitrogen and thereby completing the nitrogen cycle (22).

*Av*GReg is a soluble heme-binding protein consisting of 472 amino acids. The globin domain contains 178 amino acids and is homologous to Mb (Fig. 1*A*, see also supplemental Fig. S1 and Table S1). Based on sequence alignment, it has been proposed that the second domain of *Av*GReg is a GGDEF signaling domain of 170 amino acids (Fig. 1*B*, see also supplemental Table S2). As mentioned above, this GGDEF domain is predicted to be an enzyme in regulating second messenger levels (c-di-GMP formation) (14, 23, 24). Moreover, c-di-GMP not only regulates the expression of cellulose, as in AxPDEA1, but also stimulates the expression of adhesive curli and represses various modes of motility in *Salmonella enterica* (25, 26).

To gain insight into the molecular mechanism of signal transduction of the *Av*GReg protein and its sensor domain (*Av*GReg178), both the spectroscopic and ligand (O_2, CO, and NO) binding properties of these proteins have been investigated.

EXPERIMENTAL PROCEDURES

Cloning and Expression of AvGReg178 and AvGReg—The *A. vinelandii* strain was purchased from American Type Culture Collection (ATCC 12518). Genomic DNA was isolated using the GNOME DNA isolation kit (Qbiogene, Morgan Irvine, CA). The gene fragments of *Av*GReg178 (codons 1–178) and *Av*GReg (codons 1–472) were amplified by PCR. The PCR products were cloned into the pCR4Blunt-TOPO vector and then subcloned into pET3a. Expression of both proteins in *Escherichia coli* BL21(DE3)pLysS was performed as described previously (27).

Purification of AvGReg178—Harvesting of the cells and purification of *Av*GReg178 were mainly based on a procedure described previously (28). The expressed protein was purified from inclusion bodies. Inclusion bodies were boiled for 5 min in 50 mM Tris, pH 7.5, 6 M guanidine-HCl, 72 mM DTT, centrifuged (10,700 × *g*, 20 min at 4 °C), refolded by adding a 1.4 M excess of hemin, and dialyzed against 5 mM Tris-HCl, pH 8.5, at 4 °C. Final purification was performed by gel filtration using a Sephacryl S200 column equilibrated in 50 mM Tris, pH 8.5, 150 mM NaCl, 0.5 mM EDTA. The fractions were pooled, dialyzed against 5 mM Tris-HCl, pH 8.5, and concentrated. The samples were stored at −20 °C.

Purification of AvGReg—E. coli cells were harvested as described (27). Alternatively, the cells were resuspended in 50 mM Tris-HCl, pH 8.0, 5 mM EDTA, 1 mM phenylmethylsulfonyl fluoride. The cells were then exposed to three freeze-thaw steps and were sonicated until completely lysed. Inclusion bodies were washed two times with 50 mM Tris-HCl, pH 8.0, 5 mM EDTA, 2% sodium deoxycholate, washed once with pure water, and solubilized by incubation in 6 M guanidine-HCl, 100 mM Tris-HCl, pH 8, 72 mM DTT at a concentration of 100 mg/ml for 1 h at room temperature. After centrifugation (10,700 × *g*, 20 min., 4 °C), *Av*GReg was refolded by adding a 1.4 M excess of hemin. After an incubation time of 10 min at room temperature, the solution was diluted into 4 volumes of refolding buffer (100 mM Tris-HCl, pH 8.0, 0.2 M KCl, 0.4 M arginine, 5 mM DTT, 2% glycine) and dialyzed against the refolding buffer at 4 °C (29). Final purification was performed as described for *Av*GReg178 and checked by SDS-PAGE.

UV-visible Spectroscopy—Optical measurements were done with a Varian Cary-5 UV-visible near-infrared spectrophotometer. All UV-visible spectra were measured in the range from 200 to 800 nm.

Resonance Raman Spectroscopy—Resonance Raman (RR) measurements were carried out on a Dilor XY-800 Raman scattering spectrometer consisting of a triple 800-mm spectrograph, operating in low dispersion mode and a liquid nitrogen-cooled CCD detector. The spectra were recorded at room temperature. The excitation source was a Kr^+ ion laser (Spectra Physics 2020) at 413.1 nm. The protein solution was stirred at 600 rpm to avoid local heating and photochemical decomposition in the laser beam. Five to 10 spectra (120–300-s recording time each) were acquired to allow the removal of cosmic ray spikes. This was done by eliminating the lowest and highest data points for each frequency value and averaging the remaining values. Laser powers in the range of 1–40 milliwatts were used, as specified in the figure legends (Fig. 3 and Fig. 4).

EPR Spectroscopy—The X-band continuous wave (CW)-EPR experiments were performed on a Bruker ESP300E spectrometer (microwave frequency 9.45 GHz) equipped with a gas flow

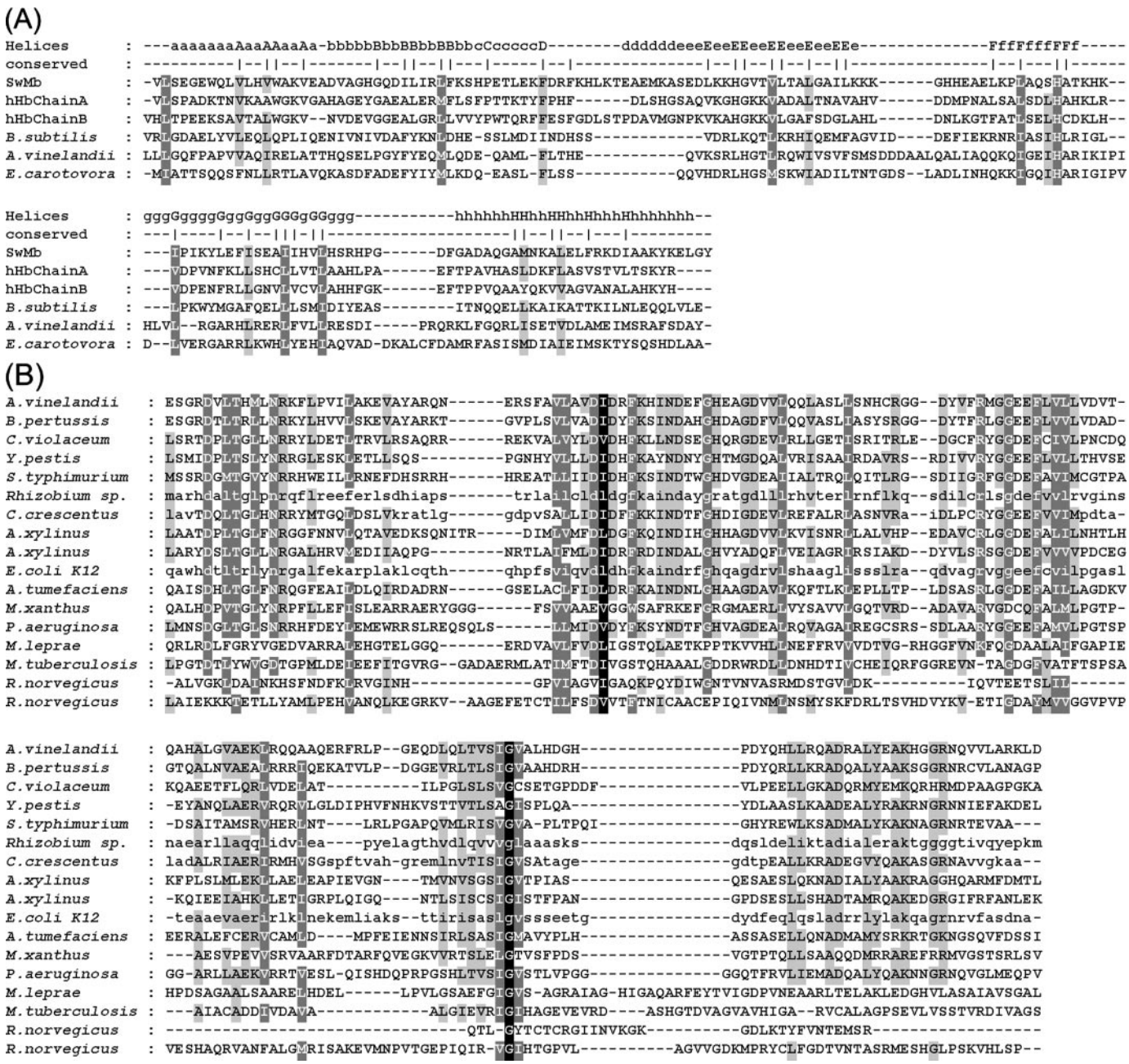

FIGURE 1. **Alignment of the GCS of *A. vinelandii* with reference molecules.** *A,* alignment of the GCS globin domain. Reference molecules are the globin domains of sperm whale Mb (*SwMb*, IA6M), human Hb chain A (*hHb* chain A, 1IRD_A), human Hb chain B (*hHb* chain B, 1IRD_B), *B. subtilis* GCS (*B. subtilis*, NP 389038), and *Erwinia carotovora* GCS (*E. carotovora*, YP_049782). *B,* alignment of the GGDEF domain. The NCBI numbers of the reference molecules are provided in supplemental data (Tables S1 and S2).

cryogenic system, allowing operation from room temperature down to 2.5 K. The magnetic field was measured with a Bruker ER035M NMR gaussmeter. The CW-EPR spectra were recorded at 10 K, a microwave power of 2 milliwatts, a modulation amplitude of 1 millitesla, and a modulation frequency of 100 kHz. The CW-EPR simulations were done with the EasySpin program, a Matlab toolbox developed for EPR simulations (30).

Carbonylation of AvGReg178 and AvGReg—Ferrous deoxygenated *Av*GReg and *Av*GReg178 (final concentration, 2.0×10^{-6} to 6.0×10^{-6} M; 0.1 M phosphate buffer, pH 7.0) was obtained by reduction of the ferric derivative with a slight excess of sodium dithionite (31). The concentrations of ferrous penta-coordinate *Av*GReg178 and of hexa-coordinate *Av*GReg were estimated using the extinction coefficients of sperm whale Mb (penta-coordinate globin) and human neuroglobin (Ngb; hexa-coordinate globin), respectively (27, 30, 31).

Kinetics of CO binding to *Av*GReg178 and *Av*GReg were determined by rapidly mixing the hemoprotein solution (final concentration, ~3.0×10^{-6} M) with the CO solution (final concentration from 1.3×10^{-5} to 4.2×10^{-4} M), at pH 7.0 (0.1 M phosphate buffer) and $T = 20.0$ °C. The CO solution was prepared by keeping in a closed vessel distilled water under CO at $p = 760.0$ torr, anaerobically ($T = 20.0$ °C). The solubility of CO

in water is 1.03×10^{-3} M at $p = 760.0$ torr and $T = 20.0$ °C (31). Then different aliquots of the CO stock solution were added to the phosphate buffer solution (final concentration, 0.1 M; pH 7.0) to obtain CO solutions containing different ligand concentrations (final concentration, 1.3×10^{-5} M to 4.2×10^{-4} M). Kinetic progress curves were monitored between 390 and 500 nm (wavelength interval = 3 nm) using the rapid mixing SX.18MV stopped-flow apparatus equipped with the PDA.1 photodiode array accessory (Applied Photophysics, Salisbury, UK). Absorbance spectra were recorded between 3 ms and 100 s on a logarithmic time base. For each CO concentration, binding kinetics were collected (at least) in triplicate and averaged.

Deoxygenation Kinetics of AvGReg178-O_2 and AvGReg-O_2—Kinetics of O_2 dissociation from oxygenated *Av*GReg and *Av*GReg178 were obtained by mixing the deoxygenated hemoprotein solutions (final concentration 3.0×10^{-6} M), in the presence of sodium dithionite (final concentration 10 mg/ml), with oxygenated pH 7 phosphate buffer solution (final concentration 0.1 M). The reaction was recorded between 3 ms and 50 s on a logarithmic time scale and monitored between 390 and 500 nm (wavelength interval = 3 nm).

Thermodynamics of AvGReg178 and AvGReg Oxygenation—O_2 equilibrium experiments were carried out with both tonometric and thin layer optical methods (28, 29).

In the tonometric method, ferrous oxygenated *Av*GReg and *Av*GReg178 (final concentration, $1–3 \times 10^{-6}$ M; 0.1 M phosphate buffer, pH 7.0) was prepared by reducing the heme-Fe atom with sodium dithionite. The excess of dithionite and by-products was removed by passing the protein solution through a Sephadex G-25 gel filtration column (Amersham Biosciences) equilibrated in air with 0.1 M phosphate buffer, pH 7.0, at 20.0 °C (31). The enzymatic Met-reducing system (32) was added to the protein solutions in the amounts detailed previously (33). O_2-binding curves were recorded at 20.0 °C by monitoring absorbance changes between 390 and 450 nm.

In the thin layer optical method, ferric *Av*GReg and *Av*GReg178 samples were reduced under anaerobic conditions by dialysis against CO-equilibrated 50 mM Hepes buffer, 0.5 mM EDTA, pH 7.6, containing 2.0 mg/ml sodium dithionite, and 1.0 mg/ml DTT (33) and stored at −80 °C as the CO derivative. Samples were thawed shortly before measurements and kept on ice until needed. Oxygen equilibrium curves of 3-μl samples were recorded at 20.0 °C by monitoring absorbance at 436 nm using a thin layer equilibration chamber fed by cascaded Wösthoff gas mixing pumps that deliver a constant flow of precise mixtures of humidified air or O_2 and ultrapure N_2 (>99.998%) (34). The samples were dissolved in 0.1 M Hepes buffer, 0.5 mM EDTA at a protein concentration of 0.3 mM heme and contained the enzymatic Met-reducing system (32) in the amounts specified previously (33). Before determination of oxygen equilibria, CO was removed from heme by repeated cycles of N_2/O_2 equilibration of the sample within the equilibration chamber until the absorbance remained constant.

Denitrosylation of AvGReg-NO and AvGReg178-NO—The *Av*GReg-NO (final concentration, 2.2×10^{-6} M) and *Av*GReg178-NO solutions (final concentration, 1.9×10^{-6} M) were prepared by reductive nitrosylation, *i.e.* by keeping overnight the buffered ferric *Av*GReg and *Av*GReg178 solutions (final concentration, 4.4×10^{-6} M and 3.8×10^{-6} M, respectively) (pH 8.3, 5.0×10^{-2} M Tricine buffer) under purified NO ($p = 760.0$ mm Hg), at 10.0 °C, under anaerobic conditions. Note that reductive nitrosylation of ferric hemeproteins is facilitated at alkaline pH values. The gaseous NO was then gently pumped off, and the *Av*GReg-NO and *Av*GReg178-NO solutions were stored without gaseous phase (35, 36) (for nitrosylation details see supplemental data S2). NO was purchased from Aldrich and purified by flowing through an NaOH column to remove acidic nitrogen oxides. The NO solution was prepared by keeping in a closed vessel the 5.0×10^{-2} M Tricine buffer solution (pH 8.3) under NO at $p = 760.0$ mm Hg, anaerobically ($T = 20.0$ °C). The solubility of NO in the aqueous buffered solution is 2.05×10^{-3} M, at $p = 760.0$ mm Hg and 20.0 °C (31, 35). All the other chemicals were purchased from Sigma and Merck. All chemicals were of analytical grade and used without purification unless stated.

Values of the first-order rate constant for NO dissociation from *Av*GReg-NO and of *Av*GReg178-NO were obtained by mixing the *Av*GReg-NO or *Av*GReg178-NO (final concentration 2.2×10^{-6} M and 1.9×10^{-6} M, respectively) solution with the CO-dithionite (final concentration, 1.0×10^{-4} M to 5.0×10^{-4} M and 1.0×10^{-2} M, respectively) solution under anaerobic conditions, at pH 8.3 (5.0×10^{-2} M Tricine buffer) and $T = 20.0$ °C. No gaseous phase was present. Kinetics was monitored spectrophotometrically between 360 and 460 nm (37).

NO-mediated Oxidation of AvGReg-O_2 and AvGReg178-O_2—Values of the pseudo-first-order rate constant for NO-mediated oxidation of *Av*GReg-O_2 and *Av*GReg178-O_2 were obtained by rapidly mixing the *Av*GReg-O_2 or *Av*GReg178-O_2 (final concentration 4.8×10^{-7} M and 4.7×10^{-7} M, respectively) solution with the NO (final concentration, 2.0×10^{-6} M to 1.6×10^{-5} M) solution, at pH 8.3 (5.0×10^{-2} M Tricine buffer) and $T = 20.0$ °C. The dead time of the SFM-400 rapid-mixing stopped-flow apparatus (Bio-Logic SAS, Claix, France) was 1.4 ms. No gaseous phase was present. Kinetics was monitored between 360 and 460 nm (35).

Data Analysis—Data were analyzed with the program Matlab 6.1 (MathWorks, Inc., South Natick, MA) and singular value decomposition (SVD) analysis. Data were fitted to Schemes 1–6 using the program GEPASI 3.30 (38–40).

The time courses for CO binding to *Av*GReg178 were fitted to the minimum reaction mechanism depicted in Scheme 1 (31),

$$\text{AvGReg178} + \text{CO} \underset{k_{\text{offCO}}}{\overset{k_{\text{onCO}}}{\longleftrightarrow}} \text{AvGReg178-CO}$$

SCHEME 1

employing Equation 1,

$$S_{\text{obsCO}} = S_{t=\infty} \pm \Delta S \times \exp^{(-k_{\text{obsCO}} \times t)} \qquad \text{(Eq. 1)}$$

where S_{obsCO} is the observed absorbance signal; $S_{t=\infty}$ is the

absorbance signal at the end of the observed process; ΔS is the absorbance change ($\pm$ symbol refers to the fact that signal can either decrease or increase); t is time, and k_{obsCO} is the observed first-order rate constant (calculations are provided in supplemental Equation S3).

Values of k_{onCO} and k_{offCO} were obtained according to Equation 2,

$$k_{obsCO} = k_{onCO} \times [CO] + k_{offCO} \quad \text{(Eq. 2)}$$

From the dependence of the total amplitude of carbonylation kinetics (proportional to the molar fraction of carbonylated *Av*GReg178; Y_{CO}) on [CO], the value of the equilibrium constant for CO binding to *Av*GReg178 (*i.e.* $K_{CO} = k_{offCO}/k_{onCO}$) was obtained according to Equation 3,

$$Y_{CO} = [CO]/(K_{CO} + [CO]) \quad \text{(Eq. 3)}$$

The time courses for CO binding to *Av*GReg could not be fitted with a single exponential, as from Equation 1a; therefore, progress curves have been fitted with the following multiexponential Equation 3,

$$S_{obs} = S_{t=\infty} \pm \sum_{i=1}^{i=n} \Delta S_i \times \exp^{(+ik_{obs} \times t)} \quad \text{(Eq. 4)}$$

where different symbols have the same meaning as in Equation 1a. The best fitting has been obtained with $n = 3$; therefore, we can describe the CO binding process to *Av*GReg by three consecutive reversible reactions according to the minimum reaction mechanism depicted in Scheme 2 (41),

$$Av\text{GReg}^{\#} \underset{k_{-1}}{\overset{k_1}{\longleftrightarrow}} Av\text{GReg}^{*} \underset{k_{onHis}}{\overset{k_{offHis}}{\longleftrightarrow}} Av\text{GReg}^{+}$$

$$Av\text{GReg}^{+} + CO \underset{k_{offCO}}{\overset{k_{onCO}}{\longleftrightarrow}} Av\text{GReg}^{+}\text{-CO}$$

SCHEME 2

where *Av*GReg$^{\#}$ is the closed hexa-coordinate form of *Av*GReg, *Av*GReg* is the open hexa-coordinate form of *Av*GReg, and *Av*GReg^{+} is the open penta-coordinate form of *Av*GReg. In particular, the different observed rate constants are defined by equations 5–7:

$$^{1}k_{obs} = k_1 + k_{-1} \quad \text{(Eq. 5)}$$

$$^{2}k_{obs} = k_{onHis} + k_{offHis} \quad \text{(Eq. 6)}$$

$$^{3}k_{obs} = k_{onCO} \times [CO] + k_{offCO} \quad \text{(Eq. 7)}$$

Therefore, $^{3}k_{obs}$ corresponds to the same event described by k_{obs} in Equation 2, and it might display similar values for the rate constants (under the assumption that the active site of the sensor domain has the same binding features when it is isolated and when it is assembled in the whole molecule). On the other hand, the accurate determination of values for individual rate constants of Equations 3 and 4 is not possible, and their values are reported in Table 1 only as estimates.

The nonlinear least square fitting of time courses of O_2 dissociation from *Av*GReg178-O_2 and *Av*GReg-O_2 was also carried out employing Equation 4, and the best fitting was obtained with $n = 2$. Therefore, in both cases we can describe the O_2 dissociation process according to the minimum reaction mechanism depicted in Scheme 3 (31),

$$Av\text{GReg178}^{+}\text{-}O_2 \xrightarrow{k^{+}_{offO2}} Av\text{GReg178}^{+} + O_2$$

$$Av\text{GReg}^{+}\text{-}O_2 \xrightarrow{k^{+}_{offO2}} Av\text{GReg}^{+} + O_2$$

$$Av\text{GReg178}^{\#}\text{-}O_2 \xrightarrow{k^{\#}_{offO2}} Av\text{GReg178}^{\#} + O_2$$

$$Av\text{GReg}^{\#}\text{-}O_2 \xrightarrow{k^{\#}_{offO2}} Av\text{GReg}^{\#} + O_2$$

SCHEME 3

where *Av*GReg178^{+} and *Av*GReg^{+} represent the "open fast" O_2 dissociation species, whereas *Av*GReg178$^{\#}$ and *Av*GReg$^{\#}$ are the "closed slow" O_2 dissociation species. In this case, because sodium dithionite does not allow the reverse leftward reactions in Scheme 3, k^{+}_{offO2} and $k^{\#}_{offO2}$ represent the dissociation rate constants of *Av*GReg178$^{\#}$-O_2 (or *Av*GReg$^{\#}$-O_2) and *Av*GReg178^{+}-O_2 (or *Av*GReg^{+}-O_2) species, respectively.

The dependence of the O_2 molar saturation fraction (Y_{O2}) of *Av*GReg178 (or *Av*GReg) on the ligand concentration (*i.e.* [O_2]) was fitted according to the minimum mechanism (Scheme 4) (31):

$$Av\text{GReg178} + O_2 \underset{}{\overset{K_{O2}}{\longleftrightarrow}} Av\text{GReg178-}O_2$$

$$Av\text{GReg} + O_2 \underset{}{\overset{K_{O2}}{\longleftrightarrow}} Av\text{GReg-}O_2$$

SCHEME 4

according to Equation 8,

$$Y_{O2} = [O_2]/(K_{O2} + [O_2]) \quad \text{(Eq. 8)}$$

where K_{O2} ($= k_{offO2}/k_{onO2} = K^{\#} = k^{\#}_{offO2}/k^{\#}_{onO2}$) is the equilibrium constant for O_2 binding to *Av*GReg178.

Values of P_{50} (*i.e.* oxygen tension at half-saturation) and n_{50} (*i.e.* Hill coefficient at half-saturation) were interpolated from the zero intercept and the slope, respectively, of Hill plots, $\log(Y/(1 - Y))$ *versus* $\log PO_2$.

The time course of NO dissociation from *Av*GReg-NO and *Av*GReg178-NO was fitted to a two-exponential process according to the minimum reaction mechanism represented by Scheme 5 (31),

$$A\nu\text{GReg}^{+}\text{-NO} + \text{CO} \xrightarrow{k^{+}_{\text{offNO}}} A\nu\text{GReg}^{+}\text{-CO} + \text{NO}$$

$$A\nu\text{GReg178}^{+}\text{-NO} + \text{CO} \xrightarrow{k^{+}_{\text{offNO}}} A\nu\text{GReg178}^{+}\text{-CO} + \text{NO}$$

$$A\nu\text{GReg}^{\#}\text{-NO} + \text{CO} \xrightarrow{k^{\#}_{\text{offNO}}} A\nu\text{GReg}^{\#}\text{-CO} + \text{NO}$$

$$A\nu\text{GReg178}^{\#}\text{-NO} + \text{CO} \xrightarrow{k^{\#}_{\text{offNO}}} A\nu\text{GReg178}^{\#}\text{-CO} + \text{NO}$$

SCHEME 5

where $A\nu$GReg^{+}-NO (or $A\nu$GReg178^{+}-NO) and $A\nu$GReg$^{\#}$-NO (or $A\nu$GReg178$^{\#}$-NO) represent the open fast and the closed slow ferrous nitrosylated species, respectively, and $A\nu$GReg^{+}-CO (or $A\nu$GReg178^{+}-CO) and $A\nu$GReg$^{\#}$-CO (or $A\nu$GReg178$^{\#}$-CO) represent the open fast and the closed slow ferrous carbonylated derivatives, respectively.

Values of k^{+}_{offNO} and $k^{\#}_{\text{offNO}}$ have been determined from data analysis, according to Equations 9 and 10 (31):

$$[A\nu\text{GReg}^{+}\text{-NO}]_t + [A\nu\text{GReg}^{\#}\text{-NO}]_t = [A\nu\text{GReg}^{+}\text{-NO}]_i \times e^{-k_{\text{offNO+}} \times t} + [A\nu\text{GReg}^{\#}\text{-NO}]_i \times e^{-k_{\text{offNO\#}} \times t} \quad \text{(Eq. 9)}$$

$$[A\nu\text{GReg178}^{+}\text{-NO}]_t + [A\nu\text{GReg178}^{\#}\text{-NO}]_t = [A\nu\text{GReg178}^{+}\text{-NO}]_i \times e^{-k_{\text{offNO+}} \times t} + [A\nu\text{GReg178}^{\#}\text{-NO}]_i \times e^{-k_{\text{offNO\#}} \times t} \quad \text{(Eq. 10)}$$

The time course of NO-mediated oxidation of $A\nu$GReg-O_2 and $A\nu$GReg178-O_2 was fitted to a two-exponential process according to the minimum reaction mechanism represented by Scheme 6 (31),

$$A\nu\text{GReg}^{+}\text{-O}_2 + \text{NO} \xrightarrow{h^{+}_{\text{on}}} \text{met}A\nu\text{GReg}^{+} + \text{NO}_3^{-}$$

$$A\nu\text{GReg178}^{+}\text{-O}_2 + \text{NO} \xrightarrow{h^{+}_{\text{on}}} \text{met}A\nu\text{GReg178}^{+} + \text{NO}_3^{-}$$

$$A\nu\text{GReg}^{\#}\text{-O}_2 + \text{NO} \xrightarrow{h^{\#}_{\text{on}}} \text{met}A\nu\text{GReg}^{\#} + \text{NO}_3^{-}$$

$$A\nu\text{GReg178}^{\#}\text{-O}_2 + \text{NO} \xrightarrow{h^{\#}_{\text{on}}} \text{met}A\nu\text{GReg178}^{\#} + \text{NO}_3^{-}$$

SCHEME 6

where met$A\nu$GReg^{+} and met$A\nu$GReg178^{+}, and met$A\nu$GReg$^{\#}$ and met$A\nu$GReg178$^{\#}$ represent the open fast and the closed slow ferric derivatives, respectively, and h_{on} represents the rate of oxidation in $\text{M}^{-1}\,\text{s}^{-1}$.

Values of h and $h^{\#}$ have been determined from data analysis, according to Equations 11 and 12 (31),

$$[A\nu\text{GReg}^{+}\text{-O}_2]_t + [A\nu\text{GReg}^{\#}\text{-O}_2]_t = [A\nu\text{GReg}^{+}\text{-O}_2]_i \times e^{-h+ \times t} + [A\nu\text{GReg}^{\#}\text{-O}_2]_i \times e^{-h\# \times t} \quad \text{(Eq. 11)}$$

$$[A\nu\text{GReg178}^{+}\text{-O}_2]_t + [A\nu\text{GReg178}^{\#}\text{-O}_2]_t = [A\nu\text{GReg178}^{+}\text{-O}_2]_i \times e^{-h+ \times t} + [A\nu\text{GReg178}^{\#}\text{-O}_2]_i \times e^{-h\# \times t} \quad \text{(Eq. 12)}$$

Values of the second-order rate constant for NO-mediated oxidation of $A\nu$GReg^{+}-O_2 or $A\nu$GReg178^{+}-O_2 (*i.e.* h^{+}_{on}) and of $A\nu$GReg$^{\#}$-O_2 or $A\nu$GReg178$^{\#}$-O_2 (*i.e.* $h^{\#}_{\text{on}}$) were estimated according to Equations 13 and 14 (31):

$$h^{+} = h_{\text{on}}{}^{+} \times [\text{NO}] \quad \text{(Eq. 13)}$$

$$h^{\#} = h^{\#}_{\text{on}} \times [\text{NO}] \quad \text{(Eq. 14)}$$

All the experiments were carried out at least in triplicate. The results are given as mean values of at least three experiments plus or minus the corresponding standard deviation.

Sequence Alignment—The globin domain sequence of the GCS of *A. vinelandii* and a selection of globin sequences were manually aligned, as described previously (42). The globin sequences used for the alignment are described in supplemental Table S1. Sequence alignment of the GGDEF domain of the GCS of *A. vinelandii* together with a selection of GGDEF sequences was performed with MUSCLE version 3.6 (43) and manually adjusted using Genedoc version 2.6 (44). The GGDEF sequences used for the alignment are described in supplemental Table S2.

RESULTS

UV-visible Spectroscopy—The optical absorption spectrum of the purified form of $A\nu$GReg178 shows the Soret maximum at 412 nm and α and β maxima at 579 and 540 nm, respectively (Fig. 2*A*). This is typical of oxygenated globins. Similar values were observed for the oxygenated derivative of *Paramecium* Hb (45) and sperm whale Mb (31). The absorption spectrum of the freshly purified form of $A\nu$GReg exhibits the Soret maximum at 410 nm and α and β maxima at 567 and 531 nm, respectively, typical for six-coordinate, low spin (LS) ferric proteins (46) (Fig. 2*B*). A very weak marker line at ~619 nm suggests that a small high spin (HS) ferric component is present. Upon addition of dithionite to $A\nu$GReg178, the absorbance maxima appear at 430 and ~560 nm. This indicates that the deoxygenated protein is in the five-coordinate, HS ferrous heme state (Fig. 2*A*) (31). The spectrum of ferrous deoxygenated $A\nu$GReg shows the Soret maximum at 421 nm and the α and β maxima at 555 and 526 nm, respectively, which is indicative of a six-coordinate LS ferrous heme iron (Fig. 2*B*). Similar UV-visible spectra were found for ferrous unliganded nonsymbiotic barley Hb (47), nonsymbiotic rice Hb (46), Ngb (27), and cytoglobin (5). The spectra are typical of globins exhibiting bis-histidine heme-Fe atom coordination. Upon CO binding to ferrous $A\nu$GReg178 and $A\nu$GReg, the Soret maximum is shifted to 421 and 416 nm, respectively. The α and β maxima of

*Av*GReg-CO are 534 and 566 nm (LS). A small band at 616 nm indicates a small fraction of an HS ferric form. The α and β maxima of *Av*GReg178-CO are situated at 540 and 570 nm.

Resonance Raman Spectroscopy—It is well established that the high frequency region of the RR spectra is composed of porphyrin in-plane modes that are sensitive to the oxidation, spin, and coordination states of the heme iron; ν_2 and ν_3 are linearly correlated with the distance between the central Fe atom and a nitrogen atom of the porphyrin ring (coordination and spin state), whereas ν_4 is sensitive to the oxidation state. In the spectrum of the as-isolated sensor domain *Av*GReg178-O_2, ν_4, ν_3, and ν_2 are located at 1372, 1502, and 1575 cm^{-1}, respectively, which are typical values of oxygenated globins (Fig. 3*B, trace a*). In the RR spectrum of the freshly purified *Av*GReg, two ν_4 bands at 1375 and ~1360 cm^{-1} and two ν_3 bands at 1506 and 1494 cm^{-1} were observed, which are indicative of a mixture of ferric and ferrous LS *Av*GReg (Fig. 3*B, trace b*). The relative intensity of these bands depends on the laser power, *i.e.* the intensity of the band at 1360 cm^{-1} (because of the ferrous heme) increases with the laser power (see supplemental Fig. S4). Therefore, this component can be assigned to the photodissociated form of the protein. This indicates that a small fraction of the protein is in the oxygenated form (the ν_4 and ν_3 frequencies of oxygenated and LS ferric hemeproteins are undistinguishable).

The deoxygenated ferrous form of *Av*GReg178 displays the ν_4, ν_3, and ν_2 bands at 1354, 1470, and 1562 cm^{-1}, respectively, typical of penta-coordinate HS ferrous hemeproteins (Fig. 3*B, trace c*). The $\nu_{Fe\text{-}His}$ stretching frequency is found to be ~220 cm^{-1}. This value is similar to the Fe-His stretching mode observed for deoxygenated Mb (220 cm^{-1}) (48). In contrast, the Fe-His stretching frequency of deoxygenated *Bacillus subtilis* HemAT (HemAT-*Bs*) was reported at a higher frequency (*i.e.* 225 cm^{-1}) (49), a feature that was related to a decrease in strain imposed on the Fe-His bond. The RR spectrum of ferrous deoxygenated *Av*GReg is clearly different, showing the ν_4, ν_3, and ν_2 bands at 1361, 1495, and 1592 cm^{-1}, respectively, which are characteristic of a six-coordinate LS ferrous heme iron (Fig. 3*B, trace d*). Accordingly, no Fe-His stretching frequency is observed in the low frequency region, confirming the hexacoordinate LS character of ferrous deoxygenated *Av*GReg. These findings reinforce the interpretation of the absorption spectroscopic data.

In the low frequency region of the RR spectra of the deoxygenated derivative, the bending mode of the heme propionate, $\delta(C_\beta C_c C_d)$, is sensitive to electrostatic interaction on the heme propionates, such as hydrogen bonds and salt bridges (50). Thus, it is recognized that the stronger the electrostatic interaction between the heme propionate and the surrounding residues, the higher is the frequency of the δ

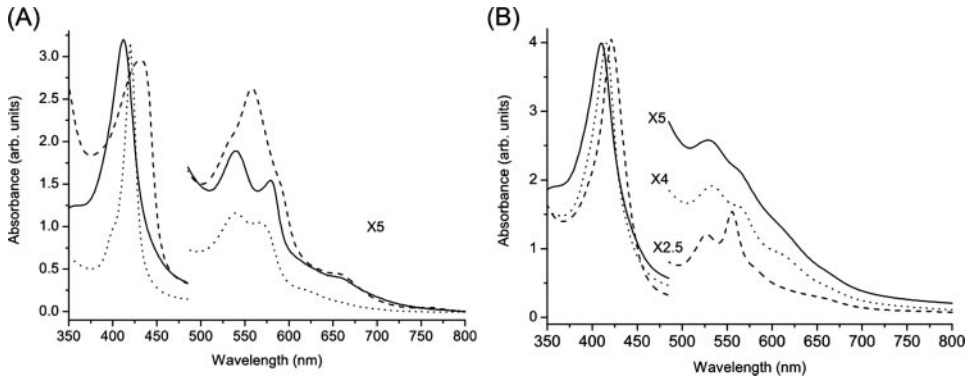

FIGURE 2. *A,* absorption spectra of *Av*GReg178. Oxygenated form (obtained after protein purification) (*continuous line*), deoxygenated form (*dashed line*), and carbonylated form (*dotted line*) are shown. *B,* absorption spectra of *Av*GReg. Ferric form (obtained after protein purification) (*continuous line*), deoxygenated form (*dashed line*), and carbonylated form (*dotted line*) are shown.

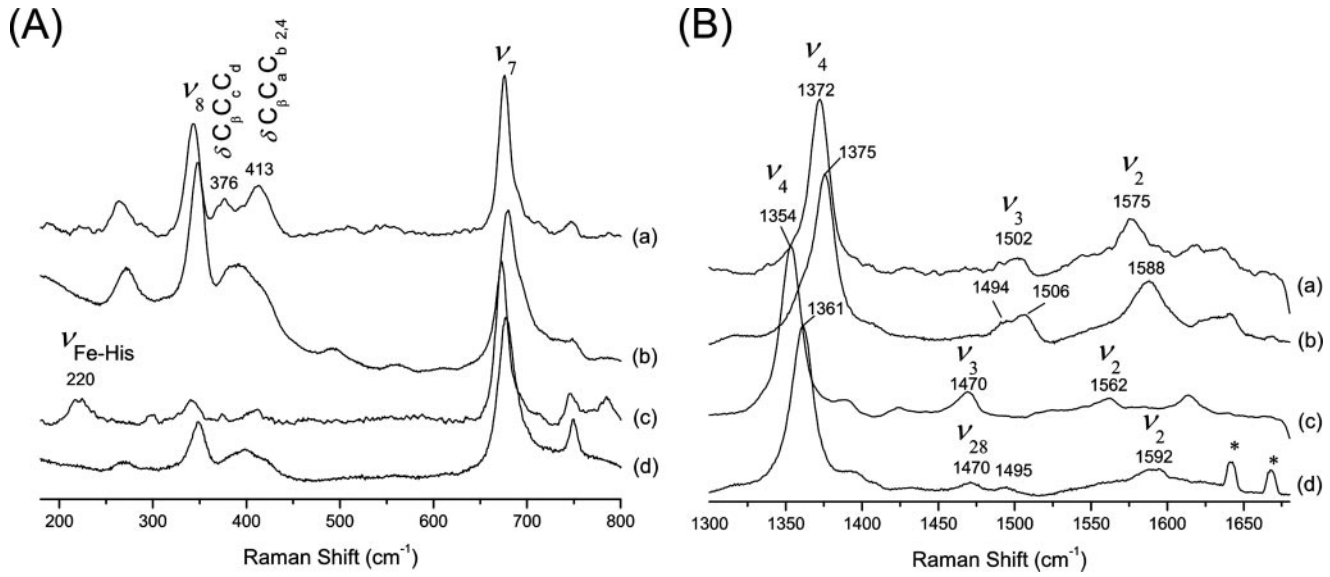

FIGURE 3. **Low frequency (*A*) and high frequency (*B*) RR spectra of purified *Av*GReg178 (oxygenated form) (*trace a*), purified *Av*GReg (ferric form) (*trace b*), ferrous *Av*GReg178 (*trace c*), and ferrous *Av*GReg (*trace d*).** The spectra were recorded at laser powers of 17 milliwatts (*traces a, c,* and *d*) and 40 milliwatts (*trace b*). The peaks indicated by * are plasma lines from the krypton laser.

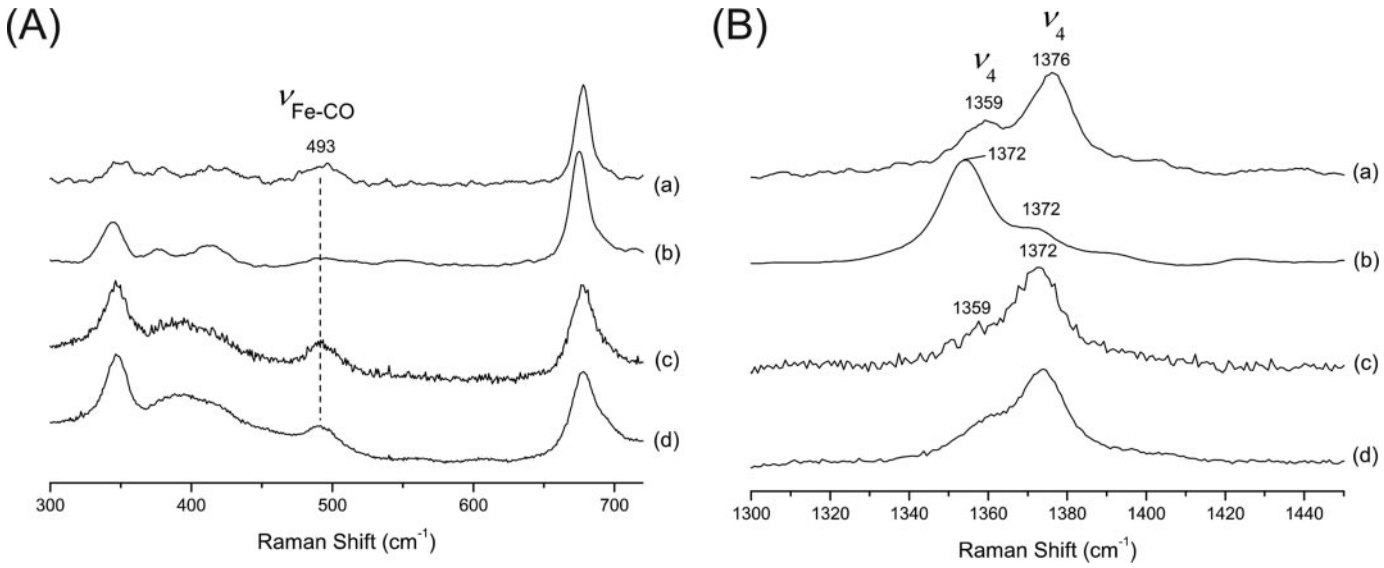

FIGURE 4. **Low frequency (*A*) and high frequency (ν_4 region) (*B*) RR spectra of the carbonylated form of *Av*GReg 178, laser power 0. 5 milliwatt (*trace a*), *Av*GReg178, laser power 1 milliwatt (*trace b*), *Av*GReg, laser power 1 milliwatt (*trace c*), and *Av*GReg, laser power, 20 milliwatts (*trace d*).**

($C_\beta C_c C_d$) band. The δ ($C_\beta C_c C_d$) bands were observed around ~374, ~379, and ~376 cm^{-1} in ferrous unliganded *Av*GReg178 (Fig. 3*A, trace c*). This is comparable with the corresponding form of Mb (371, 377, and 378 cm^{-1}, respectively), for which moderate hydrogen bonds exist on heme propionate 7 (51). The vinyl mode, δ ($C_\beta C_c C_{b2,4}$), was observed at 413 cm^{-1}. In contrast to *Av*GReg178, the propionate and vinyl modes of *Av*GReg fall together in a broad band (Fig. 3*A, trace d*). This indicates that the heme-globin contacts change significantly upon reconstitution of the full protein.

The RR spectrum of the carbonylated derivative of ferrous *Av*GReg178 reveals two ν_4 bands as follows: a dominant peak at 1376 cm^{-1} with a lower frequency shoulder (1359 cm^{-1}) (Fig. 4*B, traces a* and *b*). The shoulder at 1359 cm^{-1} stems from the HS ferrous state formed by photo-dissociation of CO. A similar, albeit smaller, photo-dissociation effect was observed for carbonylated *Av*GReg (Fig. 4*B*, *traces c* and *d*). In agreement with carbonylated HemAT-*Bs* (49) and *Paramecium* Hb (45), the ν_{Fe-CO} band of *Av*GReg178 and *Av*GReg was observed at 493 cm^{-1} (Fig. 4*A, trace d*). This frequency suggests an open conformation of the heme pocket.

EPR Spectroscopy—CW-EPR provides an excellent tool to analyze ferric hemeproteins (52). In the X-band (9.5 GHz) CW-EPR spectrum of as-isolated *Av*GReg, three different contributions could be observed stemming from one HS and two LS ferric heme forms (Fig. 5). The HS component is characterized by the principal *g* values, $g_z = 6.4$, $g_y = 5.85$, and $g_x = 1.995$, it can be ascribed to a penta-coordinate ferric form or the aquomet derivative of the sensor (53). The EPR spectra of the two LS ferric components are characterized by a highly rhombic **g** tensor. The principal *g* values of the dominant LS ferric component (LS1) are $g_z = 2.94$, $g_y = 2.28$, and $g_x = 1.52$. These *g* values can be directly related to different ligand field parameters, such as the tetragonal splitting Δ and the rhombic splitting *V*, which in turn give insight in the type of axial ligands coordinating to the heme-Fe atom (52). For the dominant LS1 component in ferric *Av*GReg, this treatment leads to the following values: $V/\lambda = 1.9$, $\Delta/\lambda = 3.21$, and $V/\Delta = 0.59$, where λ is the spin-orbit coupling. These values fall within the B region of the so-called "truth tables" of Blumberg and co-workers (54, 55), which is typical for hemeproteins with a bis-histidine heme-Fe atom coordination. This indicates that in ferric *Av*GReg, the heme iron appears to be bound to both the proximal His(F8) and distal His(E7) residues. The fact that the g_z value of LS1 is smaller than 3, combined with the value of $V/\lambda = 1.9$, hints that the two His axial ligands may be co-planar (56, 57). Comparison of *g* values obtained here with those reported by Quinn *et al.* (57), who related x-ray and CW-EPR data for five LS Fe(III) porphyrin systems with co-planar imidazoles, suggests that the angle between the projection of the His axial ligand normal on the porphyrin plane and the nearest N_p-Fe-N_p axis is ~22°.

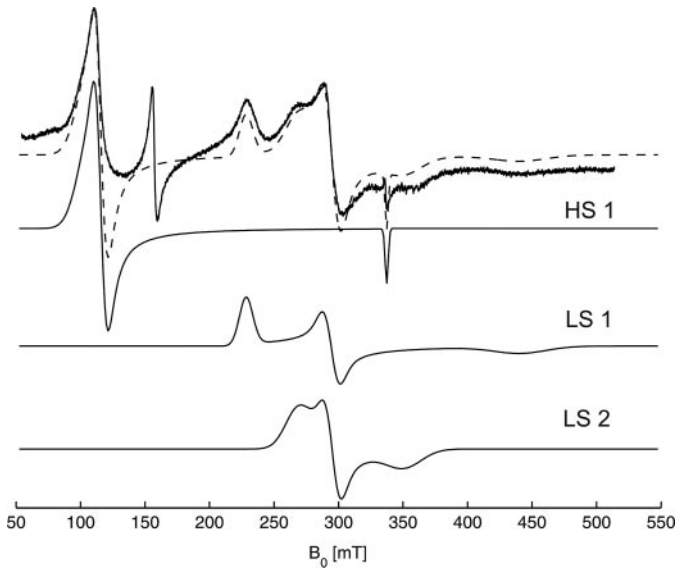

FIGURE 5. **CW-EPR spectra of ferric *Av*GReg.** Experimental (*continuous line, upper curve*) and simulations of HS1, LS1, LS2, and total (*dashed line, upper curve*).

Furthermore, a minor contribution because of a second LS ferric form (LS2) could be observed with $g_z = 2.51$, $g_y = 2.28$,

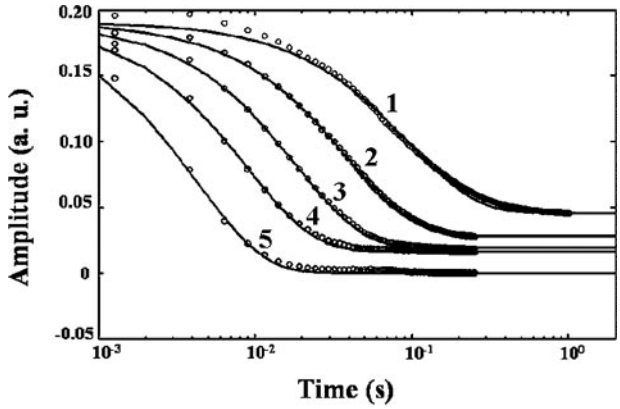

FIGURE 6. **CO binding to *Av*GReg178.** Best fit of the time courses of CO binding to *Av*GReg178 at different ligand concentrations. Over the whole CO concentration range explored (*trace 1*, [CO] = 1.3×10^{-5} M; *trace 2*, [CO] = 2.6×10^{-5} M; *trace 3*, [CO] = 5.2×10^{-5} M; *trace 4*, [CO] = 1.04×10^{-4} M; *trace 5*, [CO] = 2.08×10^{-4} M) the time course of *Av*GReg178 carbonylation conforms to single-exponential decay for more than 95% of their courses. Data have been analyzed according to Equation 1.

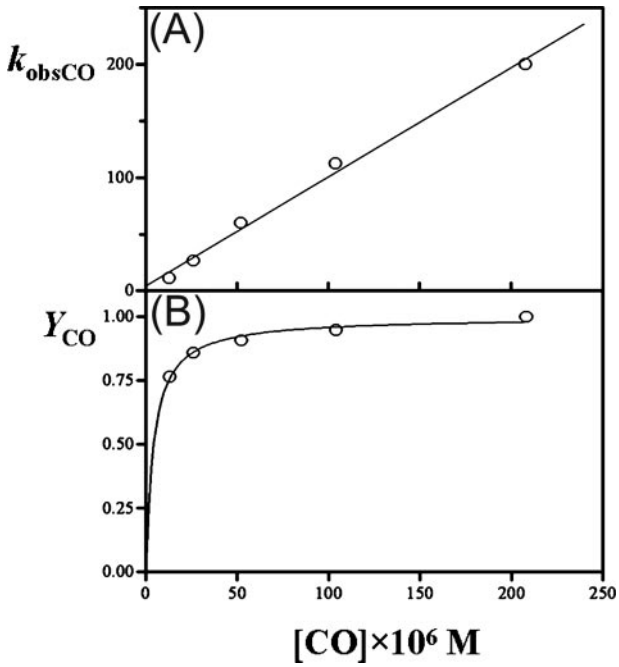

FIGURE 7. **CO binding to *Av*GReg178.** *A*, dependence of the pseudo-first-order constant (k_{obsCO}) of CO binding to the *Av*GReg178 protein on the ligand concentration. The value of the second-order rate constant for the CO binding to the *Av*GReg178 protein can be calculated from the slope of the regression line ($k_{onCO} = (1.0 \pm 0.2) \times 10^6$ M^{-1}s^{-1}), whereas the *y* intercept can give an estimate of the first-order dissociation constant ($k_{offCO} = (4.0 \pm 1.0)$ s^{-1}). *B*, molar fraction of carbonylated *Av*GReg178 (relative amplitude Y_{CO}) as a function of the ligand concentration. From data analysis the value of the dissociation equilibrium constant for CO binding to the *Av*GReg178 protein was estimated ($K_{CO} = (4.5 \pm 1.0) \times 10^{-6}$ M). *Open circles* represent experimental data whereas the *straight line* (*A*) and hyperbolic (*B*) represent the theoretical curves according to a simple CO-binding mechanism (see Scheme 1). Data in *A* have been analyzed according to Equation 2. Data in *B* have been analyzed according to Equation 3.

and $g_x = 1.91$. A component with similar principal *g* values ($g_z = 2.52$, $g_y = 2.31$, and $g_x = 1.86$) was observed in *Chlamydomonas* chloroplast Hb (58) and was assigned to heme-Fe atom coordination by the Tyr(B10) residue. The ratio LS1/LS2 is 1/2. Note that it is difficult to estimate the ratio of the HS and LS ferric species from CW-EPR spectra because of the different saturation behavior of the HS and LS EPR signals at low temperature. The absorption spectra indicate a dominance of the LS component (see Fig. 2*B*). Note that attempts to oxidize the heme iron of as-isolated *Av*GReg178 failed even after long exposure to air. This clearly marks a difference between the isolated sensorial domain and the full-length protein.

AvGReg178 and AvGReg Carbonylation Kinetics—SVD analysis of CO binding to *Av*GReg178 showed that between 390 and 500 nm only one optical transition accounts for more than 97% of the total absorbance changes (data not shown). Moreover, over the whole CO concentration range explored, the time course of the *Av*GReg178 carbonylation conforms to a single-exponential decay for more than 95% of its course, being in pseudo-first-order conditions (Fig. 6). Therefore, the minimum reaction mechanism depicted by Scheme 1 was employed to determine kinetic parameters for CO binding to *Av*GReg178. Data analysis carried out with fitting procedures allowed determination of the following kinetic parameters: $k_{onCO} = (1.0 \pm 0.2) \times 10^6$ M^{-1} s^{-1} and $k_{offCO} = (4.0 \pm 1.0)$ s^{-1} (pH 7.0 and T = 20.0 °C). They are in good agreement with the estimates from the plot of observed pseudo-first-order rate constant (k_{obsCO}) as a function of CO concentration (Fig. 7*A*). Values of the molar fraction of carbonylated *Av*GReg178 ($Y_{CO} = A^{obs}/A_{max}$ at each wavelength) are wavelength-independent. The plot of Y_{CO} *versus* [CO] is hyperbolic with $K_{CO} = (4.5 \pm 1.0) \times 10^{-6}$ M (Fig. 7*B*; see Equation 3), which is in excellent agreement with the value of K_{CO} ($= k_{offCO}/k_{onCO}$ for a penta-coordinate form) = $(4 \pm 2) \times 10^{-6}$ M calculated from values of k_{onCO} and k_{offCO}, as expected from Scheme 1.

For *Av*GReg, SVD analysis showed that between 390 and 500 nm only one optical transition accounts for more than 90% of the total absorbance changes (data not shown). However, over the whole CO concentration range explored, the time course for *Av*GReg carbonylation does not conform to a single-exponential decay but rather to a multiphase process (Fig. 8). The minimum reaction mechanism describing the experimental data demands three consecutive reversible reactions (see Scheme 2). If we assume that the active site of the globin domain of the full molecule has the same binding features of *Av*GReg178,

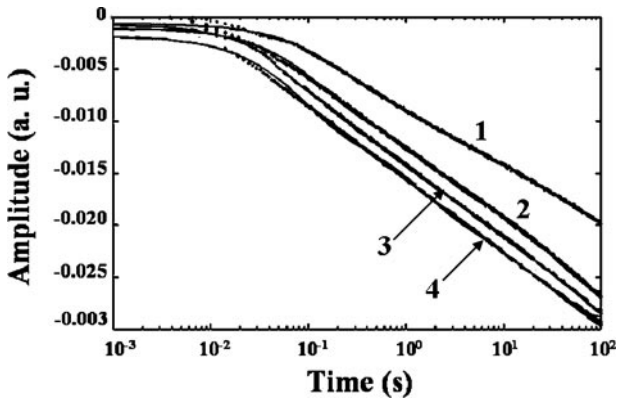

FIGURE 8. **CO binding to *Av*GReg.** Best fit of the time course of CO binding to *Av*GReg at different ligand concentrations (*trace 1*, [CO] = 1.3×10^{-5} M; *trace 2*, [CO] = 2.6×10^{-5} M; *trace 3*, [CO] = 5.2×10^{-5} M; *trace 4*, [CO] = 4.2×10^{-4} M). The *continuous lines* were obtained from the fitting procedure carried out with GEPASI on the basis of the Scheme 2 (for details see text). The percentage of the fast, middle, and slow phase was 33 ± 4%.

TABLE 1
Rate and equilibrium constants for ligand binding

	His					CO				O_2			P_{50}	
	k_{onHis}	k_{offHis}	K_{His}	k_1	k_{-1}	k_{offHis}	k_{onHis}	k_{onCO}	k_{offCO}	$K_{pentaCO}$[a]	k_{onO2}	k_{offO2}	$K_{pentaO2}$[a]	K_{hexaO2}[b]	measured	Ref.
	s^{-1}	s^{-1}		s^{-1}	s^{-1}	s^{-1}	s^{-1}	$M^{-1}\,s^{-1}\times 10^6$	s^{-1}	μM	$M^{-1}\,s^{-1}\times 10^6$	s^{-1}	μM	μM	*torr*	
SwMb wild type								0.5	0.019	0.038	5.3	10	1.887		0.51	103, 104
*Av*GReg178								1	4	4.5	424	10.6	0.025		0.04	This study
										4	5.2	0.13[c]	0.025			
*Av*GReg	≤0.5	2.8	≥5.6	0.1	≤0.01	2.8	≤0.5	1	4	4		10.6		0.12	0.15	This study
												0.73[c]		0.12		
HemAT-*Bs* (sensor domain)								0.43	0.07	0.16	19	1800	94 to 74			105
												50				
HemAT-*Bs*								0.34	0.067	0.20	19	1900	100		0.1	105
												87				
HNgb	2000	4.5	0.002					65	0.014	0.00022	250	0.8	0.003	0.70	2.6	33
MNgb	1000	0.5	0.0005					55			200	0.4	0.002	0.25	2.2	83
Rice Hb								7.2	0.001	0.00014	68	0.038	0.001			46
Human cytoglobin + DTT	200	2	0.01					5			27	0.9	0.033	0.30		83
Paramecium Hb								27.7	0.328	11.8	30.1	25.2	0.837		0.45	45

[a] Values of the dissociation constants (k_{off}/k_{on}).
[b] K_{hexaO2} was calculated as follows: $K_{hexaO2} = (K_{O2dis}{}^{-1}/(1 + K_{His}{}^{-1}))$.
[c] Values of the closed slow conformation.

FIGURE 9. **Time courses of O_2 dissociation from *Av*GReg178-O_2 (*trace 1*) and *Av*GReg-O_2 (*trace 2*).** *Points* represent experimental data. *Continuous lines* were obtained by the two independent exponential data analysis according to Scheme 3. Values of k_{offO2} and $k^{\#}{}_{offO2}$ for *Av*GReg178 and *Av*GReg are $k_{offO2} = 10.6 \pm 0.7\ s^{-1}$, $k^{\#}{}_{offO2} = 0.13 \pm 0.04\ s^{-1}$, $k_{offO2} = 10.6 \pm 0.8\ s^{-1}$, and $k^{\#}{}_{offO2} = 0.73 \pm 0.04\ s^{-1}$, respectively. The percentages of the fast and slow phases were 31 and 69% for *Av*GReg178, and 48 and 52% for *Av*GReg, respectively. Both time courses start at −0.08 absorbance units (*a.u.*).

then data fitting analysis can be carried out fixing values of k_{onCO} and k_{offCO} to those obtained from *Av*GReg178 for the bimolecular CO binding rate constant (see Schemes 1 and 2). This allowed us to determine the remaining kinetic parameters (see Scheme 2), for some of which (namely k_{-1} and k_{-2}) only the upper limiting values were obtained, *i.e.* $k_1 = 0.1 \pm 0.01\ s^{-1}$, $k_{-1} \leq 0.01\ s^{-1}$, $k_{offHis} = 2.8 \pm 0.2\ s^{-1}$, and $k_{onHis} \leq 0.5\ s^{-1}$ (pH = 7.0 and T = 20.0 °C).

Values of kinetic and thermodynamic parameters for *Av*GReg178 and *Av*GReg carbonylation are shown in Table 1, where they are compared with those of globins. A striking observation is the fact that for both *Av*GReg178 and *Av*GReg the CO dissociation constant k_{off} is ~200-fold faster than for sperm whale Mb, whereas the CO association rate constants are similar (see Table 1).

AvGReg178 and AvGReg Oxygen Dissociation Kinetics—SVD analysis concerning kinetics of O_2 dissociation from oxygenated *Av*GReg178 and *Av*GReg showed that between 390 and 500 nm only one optical transition accounts for more than 98 and 90%, respectively, of the total absorbance changes. The time course of O_2 dissociation from *Av*GReg178-O_2 and *Av*GReg-O_2 was fitted with a two-phase exponential decay (see Fig. 9). The biphasic time course of *Av*GReg178 and of *Av*GReg represents O_2 dissociation from the open fast (*Av*GReg$^+$ and *Av*GReg178$^+$) and closed slow (*Av*GReg$^{\#}$ and *Av*GReg178$^{\#}$) species (see Scheme 3).

The data fitting analysis was carried out fixing the value of the fast phase (*i.e.* open fast) of the time course of deoxygenation kinetics (*i.e.* k_{offO2}) of *Av*GReg178-O_2 and *Av*GReg-O_2 (see Scheme 3). Values of the dissociation constants of the open fast ($k^+{}_{offO2}$) and of the closed slow ($k^{\#}{}_{offO2}$) oxygenated derivatives of *Av*GReg178 are $k^+{}_{offO2} = 10.6 \pm 0.7\ s^{-1}$ and $k^{\#}{}_{offO2} = 0.13 \pm 0.04\ s^{-1}$ and of *Av*GReg are $k^+{}_{offO2} = 10.6 \pm 0.8\ s^{-1}$ and $k^{\#}{}_{offO2} = 0.73 \pm 0.04\ s^{-1}$. Values of kinetic parameters $k^+{}_{offO2}$ and $k^{\#}{}_{offO2}$ for *Av*GReg178 and *Av*GReg deoxygenation are shown in Table 1.

AvGReg178 and AvGReg Oxygen Equilibrium Measurements—Fig. 10 shows the isotherms for O_2 binding to *Av*GReg178 and

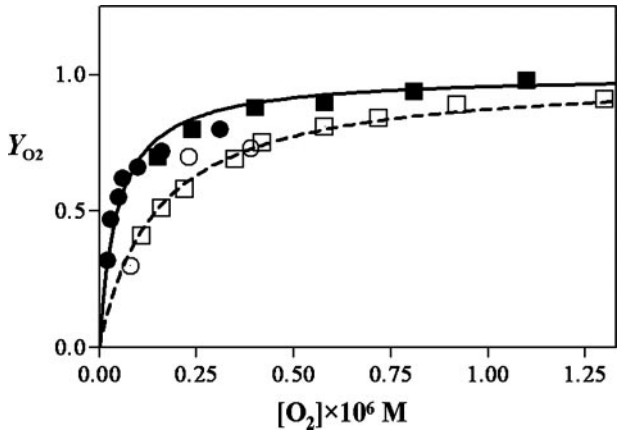

FIGURE 10. **O_2 equilibrium measurements carried out at 20.0 °C with the tonometric method (*squares*) and the thin layer optical method (*circles*) to *Av*GReg178 (*filled symbols*) and to *Av*GReg (*open symbols*).** Data obtained with the two methods were analyzed as a unique data set on the basis of Equation 8. Values of $K_{O2} = K^{\#}_{O2}$ for *Av*GReg178 and *Av*GReg oxygenation are $(2.5 \pm 1.3) \times 10^{-8}$ M) and $(1.2 \pm 0.4) \times 10^{-7}$ M), respectively. Values of P_{50} for *Av*GReg178 and *Av*GReg oxygenation are 0.04 and 0.15 torr, respectively.

*Av*GReg as obtained by the tonometric and the thin layer optical methods. Both proteins display a high affinity for O_2 ($K_{O2} = K^{\#}_{O2} = (2.5 \pm 1.3) \times 10^{-8}$ M for *Av*GReg178 and $K_{O2} = K^{\#}_{O2} = (1.2 \pm 0.4) \times 10^{-7}$ M for *Av*GReg) with P_{50} values of 0.04 torr for *Av*GReg178 and 0.15 torr for *Av*GReg.

Values of K_{O2} for *Av*GReg178 and *Av*GReg oxygenation are an average of tonometric and thin layer results. Binding isotherms for both *Av*GReg178 and *Av*GReg could be fitted satisfactorily employing a single equilibrium binding constant, although experiments on *Av*GReg178 by the thin layer method could be better fitted implying slight apparent negative cooperativity ($n \cong 0.8$), which appears consistent with the functional heterogeneity observed in oxygen dissociation kinetics. In any event, this result clearly demonstrates that for the two proteins, the open fast (characterized by K^{+}_{O2}) and the closed slow species (characterized by $K^{\#}_{O2}$) display a similar binding affinity. Therefore, the biphasic O_2 dissociation kinetics (*i.e.* $k^{+}_{offO2} \neq k^{\#}_{offO2}$) implies also a biphasic O_2 association process (*i.e.* $k^{+}_{onO2} \neq k^{\#}_{onO2}$), which partially compensates, resulting in closely similar affinity (*i.e.* $K^{+}_{O2} \cong K^{\#}_{O2}$). As a consequence, values of k^{+}_{onO2} and $k^{\#}_{onO2}$ were roughly estimated for *Av*GReg178 from values of K^{+}_{O2}, k^{+}_{offO2}, and $k^{\#}_{offO2}$, according to Scheme 4. However, for *Av*GReg, a hexa-coordinate globin, this extrapolation cannot be done because the affinity for the internal histidine cannot be ignored. Values of thermodynamic parameters for *Av*GReg178 and *Av*GReg oxygenation are shown and compared with those reported for sperm whale Mb in Table 1. It clearly emerges that the closed slow conformation of *Av*GReg178 displays a value for $k^{\#}_{onO2}$ similar to the association rate constant for sperm whale Mb, whereas the dissociation rate constants $k^{\#}_{offO2}$ are much slower than for sperm whale Mb. On the other hand, in the case of the open fast conformation the opposite is found, whereby a close similarity with sperm whale Mb is observed for the dissociation rate constant k_{offO2}, whereas a much faster O_2 association rate constant is observed for *Av*GReg178 (Table 1).

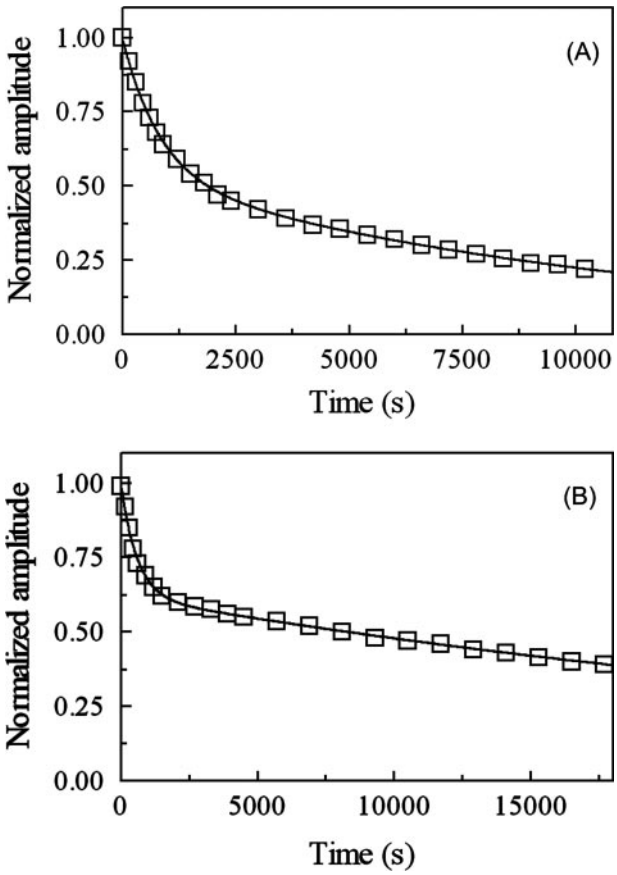

FIGURE 11. **NO dissociation from *Av*GReg-NO and *Av*GReg178-NO.** *A*, normalized averaged time courses of NO dissociation from *Av*GReg^{+}-NO and *Av*GReg$^{\#}$-NO. The time course analysis according to Equation 9 allowed determination of $k^{+}_{offNO} = 1.2 \times 10^{-3}$ s^{-1} and $k^{\#}_{offNO} = 8.6 \times 10^{-5}$ s^{-1}. *B*, normalized averaged time courses for NO dissociation from *Av*GReg178^{+}-NO and *Av*GReg178$^{\#}$-NO. The time course analysis according to Equation 9 allowed us to determine $k^{+}_{offNO} = 1.7 \times 10^{-3}$ s^{-1} and $k^{\#}_{offNO} = 2.5 \times 10^{-5}$ s^{-1}. Spectra were collected every 5 min. The CO and dithionite concentrations were 5.0×10^{-4} and 1.0×10^{-2} M, respectively. The *Av*GReg-NO and *Av*GReg178-NO concentrations were 2.2×10^{-6} and 1.9×10^{-6} M, respectively. All data were obtained at pH 8.3 (5.0×10^{-2} M Tricine buffer) and T = 20.0 °C.

AvGReg-NO and AvGReg178-NO Denitrosylation—Over the wavelength and [CO] ranges explored, the time course for NO dissociation from *Av*GReg-NO and *Av*GReg178-NO conforms to a two-exponential process for more than 90% of its course (Fig. 11). Values of the first-order rate constant for NO dissociation from *Av*GReg^{+}-NO ($k^{+}_{offNO} = 1.2 \times 10^{-3}$ s^{-1}) and *Av*GReg$^{\#}$-NO ($k^{\#}_{offNO} = 8.6 \times 10^{-5}$ s^{-1}) as well as from *Av*GReg178^{+}-NO ($k^{+}_{offNO} = 1.7 \times 10^{-3}$ s^{-1}) and *Av*GReg178$^{\#}$-NO ($k^{\#}_{offNO} = 2.5 \times 10^{-5}$ s^{-1}), at pH 8.3 and 20.0 °C, are wavelength- and [CO]-independent in the presence of dithionite excess (data not shown).

Values of the first-order rate constant for NO dissociation from heme-NO-proteins (*i.e.* k_{offNO}) span over 3 orders of magnitude (Table 2) (59–66), reflecting structurally different stabilization mode(s) of the heme-bound NO by heme distal residue(s).

NO-mediated Oxidation of AvGReg-O_2 and AvGReg178-O_2—NO induces the oxidation of hemoproteins, and this process is postulated to depend on the superoxide character of the heme-bound O_2 (35, 67–74). Over the wavelength range explored, the

TABLE 2
Values of k_{offNO} for denitrosylation of heme-Fe(II)-NO proteins

Heme-Fe(II)-NO protein	k_{offNO} (s^{-1})	Conditions	Ref.
*Av*GReg^{+}	1.2×10^{-3}	pH 8.3 and 20.0 °C	This study
*Av*GReg$^{\#}$	8.6×10^{-5}	pH 8.3 and 20.0 °C	This study
*Av*GReg178^{+}	1.7×10^{-3}	pH 8.3 and 20.0 °C	This study
*Av*GReg178$^{\#}$	2.5×10^{-5}	pH 8.3 and 20.0 °C	This study
G. max legHb	2.0×10^{-5}	pH 7.0 and 20.0 °C	64
SwMb	1.0×10^{-4}	pH 7.0 and 20.0 °C	63
Horse heart Mb	1.0×10^{-4}	pH 7.4 and 20.0 °C	65
Human soluble guanylyl cyclase	6.0×10^{-4}	pH 8.3 and 24.0 °C	66
Mouse Ngb	2.0×10^{-4}	pH 7.5 and 25 °C	62
Rabbit hemopexin-heme	9.1×10^{-4}	pH 7.0 and 10.0 °C	60
Human Hb, R-state, α-chains	1.6×10^{-4}	pH 7.2 and RT[a]	61
β-chains	8.0×10^{-5}	pH 7.2 and RT	61
Human Hb, T-state, α-chains	4.4×10^{-3}	pH 7.2 and RT	61
β-chains	9.4×10^{-5}	pH 7.2 and RT	61
M. leprae trHbO	1.3×10^{-4}	pH 7.0 and 20.0 °C	59
E. coli flavo-Hb	2.0×10^{-4}	pH 7.0 and 20.0 °C	76

[a] RT indicates room temperature.

time course for NO-mediated oxidation of *Av*GReg-O_2 and *Av*GReg178-O_2 conforms to a two-exponential process for more than 90% of its course, at [NO] = 2.0×10^{-6} M and 4.0×10^{-6} M (Fig. 2*A*). At [NO] ≥ 8.0×10^{-6} M, kinetics was essentially mono-exponential, because the time course of NO-mediated oxidation of *Av*GReg^{+}-O_2 and *Av*GReg178^{+}-O_2 was lost in the dead time of the rapid-mixing stopped-flow apparatus, and the observed trace only reflects NO-mediated oxidation of *Av*GReg$^{\#}$-O_2 (Fig. 12*A*) and *Av*GReg178$^{\#}$-O_2 (data not shown). Values of the pseudo-first-order rate constant for NO-mediated oxidation of *Av*GReg^{+}-O_2 and *Av*GReg178^{+}-O_2 (*i.e.* h^{+}) and of *Av*GReg-O_2 and *Av*GReg178-O_2 (*i.e.* $h^{\#}$) are wavelength-independent at fixed [NO]. The plot of h^{+} and $h^{\#}$ *versus* [NO] is linear with a *y* intercept at 0, the slope corresponding to values of the second-order rate constant for NO-mediated oxidation of *Av*GReg^{+}-O_2 and *Av*GReg178^{+}-O_2 ($h_{on}{}^{+}$ = 3.2×10^{7} M^{-1} s^{-1} and 4.6×10^{7} M^{-1} s^{-1}, respectively) and *Av*GReg$^{\#}$-O_2 and *Av*GReg178$^{\#}$-O_2 ($h_{on}{}^{\#} = 2.5 \times 10^{6}$ M^{-1} s^{-1} and 7.2×10^{5} M^{-1} s^{-1}, respectively) (Fig. 12*B* and Table 3). As already reported for *Glycine max* legHb, horse heart Mb, human Hb, murine Ngb, *Mycobacterium tuberculosis* trHbN and trHbO, and *E. coli* flavoHb (35, 75–80), NO-mediated oxidation of *Av*GReg$^{\#}$-O_2 and *Av*GReg178$^{\#}$-O_2 appears to be limited by the formation of the heme-Fe(III)-peroxynitrite intermediate, which does not accumulate. In fact, the first-order process (*i.e.* independent of [NO]) representing dissociation and isomerization of peroxynitrite, which otherwise would follow the pseudo-first-order step (35), is undetectable in NO-mediated oxidation of *Av*GReg$^{\#}$-O_2 and *Av*GReg178$^{\#}$-O_2 (see Fig. 12*A*). NO-mediated oxidation of *Mycobacterium leprae* trHbO(II)-O_2 represents an exception, the dissociation and isomerization of peroxynitrite representing the rate-limiting step (81).

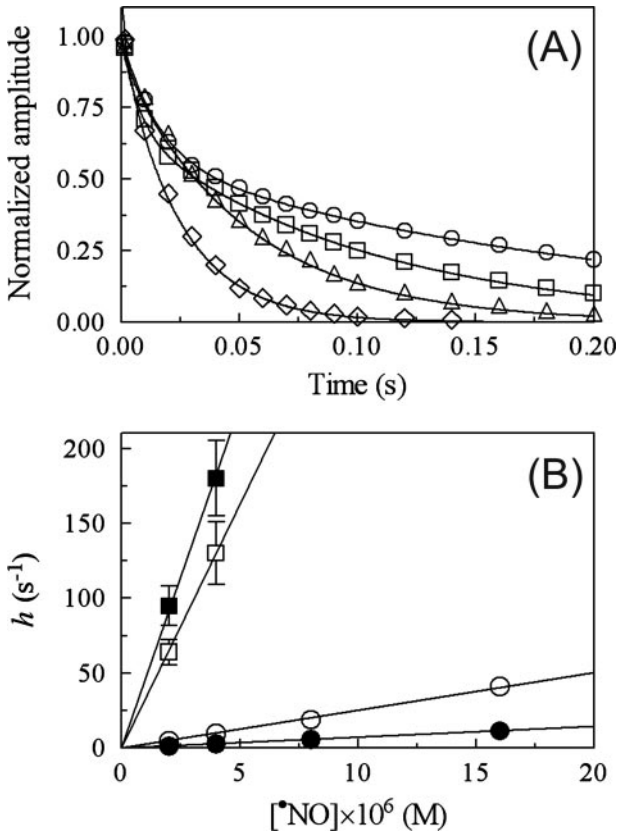

FIGURE 12. **NO-mediated oxidation of *Av*GReg-O_2 and *Av*GReg178-O_2.** *A,* normalized averaged time courses for NO-mediated oxidation of *Av*GReg^{+}-O_2 and *Av*GReg$^{\#}$-O_2. The time course analysis according to Equation 10 allowed the determination of $h^{+} = 6.4 \times 10^{1}$ s^{-1} and $h^{\#} = 4.8$ s^{-1} at [NO] = 2.0×10^{-6} M (*circles*), $h^{+} = 1.3 \times 10^{2}$ s^{-1} and $h^{\#} = 9.9$ s^{-1} at [NO] = 4.0×10^{-6} M (*squares*), $h^{\#} = 1.9 \times 10^{1}$ s^{-1} at [NO] = 8.0×10^{-6} M (*triangles*), and $h^{\#} = 4.1 \times 10^{1}$ s^{-1} at [NO] = 1.6×10^{-5} M (*diamonds*). The time course of NO-mediated oxidation of *Av*GReg^{+}-O_2 was essentially undetectable at [NO] ≥ 8.0×10^{-6} M. The *Av*GReg-O_2 concentration was 4.8×0^{-7} M. *B,* dependence of h^{+} and $h^{\#}$ values (*squares* and *circles*, respectively) on the NO concentration for NO-mediated oxidation of *Av*GReg-O_2 (*open symbols*) and *Av*GReg178-O_2 (*filled symbols*). Data analysis according to Equations 11 and 12 allowed us to determine the following values of $h_{on}{}^{+} = 3.2 \times 10^{7}$ M^{-1} s^{-1} and $h_{on}{}^{\#} = 2.5 \times 10^{6}$ M^{-1} s^{-1} for NO-mediated oxidation of *Av*GReg-O_2, and of $h_{on}{}^{+} = 4.6 \times 10^{7}$ M^{-1} s^{-1} and $h_{on}{}^{\#} = 7.2 \times 10^{5}$ M^{-1} s^{-1} for NO-mediated oxidation of *Av*GReg178-O_2. The *Av*GReg-O_2 and *Av*GReg178-O_2 concentration was 4.8×10^{-7} and 4.7×10^{-7} M, respectively. All data were obtained at pH 8.3 (5.0×10^{-2} M Tricine buffer) and $T = 20.0$ °C.

TABLE 3
Values of k_{on} for NO-mediated oxidation of heme-Fe(II)-O_2 proteins

Heme-Fe(II)-O_2-protein	h_{on} (M^{-1} s^{-1})	Conditions	Ref.
*Av*GReg^{+}	3.2×10^{7}	pH 8.3 and 20.0 °C	This study
*Av*GReg$^{\#}$	2.5×10^{6}	pH 8.3 and 20.0 °C	This study
*Av*GReg178^{+}	4.6×10^{7}	pH 8.3 and 20.0 °C	This study
*Av*GReg178$^{\#}$	7.2×10^{5}	pH 8.3 and 20.0 °C	This study
G. max legHb	8.2×10^{7}	pH 7.3 and 20.0 °C	78
Horse heart Mb	4.4×10^{7}	pH 7.0 and 20.0 °C	77
Mouse Ngb	$>7.0 \times 10^{7}$	pH 7.0 and 20.0 °C	75
Human Hb	8.9×10^{7}	pH 7.0 and 20.0 °C	77
M. tuberculosis trHbN	7.5×10^{8}	pH 7.5 and 23.0 °C	79
M. tuberculosis trHbO	6.0×10^{5}	pH 7.5 and 23.0 °C	80
M. leprae trHbO	2.1×10^{6}	pH 7.3 and 20.0 °C	81
E. coli flavoHb	$\geq 6 \times 10^{8}$	pH 7.0 and 20.0 °C	76

DISCUSSION

Both recombinant full-length *Av*GReg and its sensor domain *Av*GReg178 were successfully expressed in *E. coli* BL21(DE3)pLysS cells. There was no evidence that *Av*GReg and the products of this protein were toxic for the cells, although Ryjenkov *et al.* (24) proposed that the products of the enzymatic reaction of the GGDEF domain (*i.e.* c-di-GMP) are cytotoxic. This can be explained by the fact that *Av*GReg was

expressed in inclusion bodies, and there was probably no formation of c-di-GMP. Reconstitution of the globin domain had to be completed *in vitro* by the addition of 1.4 M excess of hemin. No additional cofactors were added for the refolding of the second domain based on procedures found in the literature (82). In contrast with Hecht *et al.* (82), $MgCl_2$ was not added although it is important for the activation of the GGDEF domain.

Physiological Significance—The heme in *Av*GReg is thought to play an important role for sensing O_2 or other ligands. The nature of the ligand, the interaction between the heme-Fe-bound ligand and heme distal amino acid residues, and/or the heme geometry could be responsible for triggering the signal transduction pathway upon ligand binding to the heme in *Av*GReg. A study of the heme-pocket structure is therefore important to elucidate the mechanism of ligand binding and signal triggering. Absorption and RR spectroscopy observations show that the heme coordination number of ferrous *Av*GReg178 changes upon ligand binding (five-to-six-coordination). In contrast, the heme coordination number of ferrous full-length protein *Av*GReg does not change upon binding of an effector molecule, as it remains hexa-coordinate. This indicates that, unlike in the globin domain *Av*GReg178, binding of an exogenous ligand to the full-length protein brings about the dissociation and displacement of the endogenous heme distal His residue; this event may trigger conformational changes in the protein. More subtle processes, such as hydrogen bonding formation between the heme-bound effector molecule and the surrounding amino acid residues, as proposed for O_2-bound HemAT-*Bs* (but not for CO- and NO-bound HemAT-*Bs*) (18), may play a critical role.

Interestingly, ferrous carbonylated *Av*GReg178 and *Av*GReg exhibit the $\nu_{Fe\text{-}CO}$ band at 493 cm^{-1} (Fig. 4*A*, *traces c* and *d*), indicating that the environment of the heme-bound CO is similar in the full protein and in the globin domain. Indeed, this could justify our assumption that the intrinsic bimolecular CO binding rate constant (*i.e.* k_{on} in Schemes 1 and 2) and the CO dissociation rate constant (*i.e.* k_{off} in Schemes 1 and 2) are the same for both *Av*GReg178 and *Av*GReg (Table 1). The difference between the sensor domain and the full protein resides then in the pathway for the ligand access to the reaction center, which is quite open for the sensor domain, whereas in the full protein the additional domain(s) hide(s) the heme pocket and the access of the ligand is permitted only through a series of conformational changes. The observed stretching frequency is typical of a conformation in which CO has very little polar interaction with the surrounding amino acids (open conformation of the heme pocket). This suggests that the displaced heme distal His(E7) in *Av*GReg does not interact with the Fe-bound CO. This contrasts with the observations for the bis-histidine coordinate heme-Fe atom in Ngb (84) and cytoglobin (5), for which CO ligation induces a mixture of open and closed conformations. On the other hand, these spectroscopic features are similar to those displayed by the CO-ligated forms of HemAT-Bs (18) and *Paramecium* Hb (45) but differ from observations concerning mammalian Mb (85).

Unlike the Fe-CO frequencies, those corresponding to the heme vinyl and propionate modes show significant differences between *Av*GReg178 and *Av*GReg (Fig. 3*A*). Because the frequency of the propionate bending mode $\delta(C_\beta C_c C_d)$ is indicative of hydrogen bonding between the heme-7-propionate group and the surrounding amino acid residues, low frequencies observed for *Av*GReg178 indicate weak (or no) heme-7-propionate hydrogen bonding for the globin domain. However, the propionate and vinyl groups of the full-length protein fall together in a broad band, suggesting that the conformation of the heme group changes significantly upon reconstitution of the full-length protein. This can mean that the activation of the second domain depends on hydrogen bonding with heme peripheral groups. Indeed, it accounts for the different structure of the heme pocket of the sensor domain depending on whether the second domain is present (as in *Av*GReg) or not (as in *Av*GReg178). The comparison of the globin domain and the whole molecule clearly shows differences, and as such, only the whole molecule is physiologically relevant.

Selective Ligand Binding—The data reported here indicate that *Av*GReg178 displays Mb-like spectroscopic properties. However, *Av*GReg178 and *Av*GReg display different functional behaviors. In fact, *Av*GReg178 follows Mb-like functional properties (86) (see Scheme 1), whereas *Av*GReg displays three-phasic reaction kinetics reminiscent of that reported for hexa-coordinate hemoproteins (41) (Scheme 2). Thus, the low reactivity of the *Av*GReg hemoprotein may reflect the conversion of the *Av*GReg[§] closed, hexa-coordinate species to the *Av*GReg* open, hexa-coordinate form that in turn converts to the *Av*GReg open, penta-coordinate species. Only the last-mentioned species reacts with CO leading to *Av*GReg $^+$-CO (Scheme 2). The data analysis indicates that *Av*GReg178 and *Av*GReg could share the same intrinsic reactivity toward CO (*i.e.* $k_{onCO} = (1.0 \pm 0.2) \times 10^6\ M^{-1}\ s^{-1}$ and $k_{offCO} = (4.0 \pm 1.0)\ s^{-1}$), as also suggested by the closely similar spectroscopic features of the CO-bound form (see above and Fig. 4*A*). Therefore, the non-heme domain of *Av*GReg lowers the CO reactivity, stabilizing the hexa-coordinate species of the heme domain (see Scheme 2). The CO binding behavior of *Av*GReg mirrors the close similarity between the absorption spectrum in the Soret region of the deoxygenated derivative of the *Av*GReg hemoprotein (Fig. 2*B*) and that of hexa-coordinate bis-histidyl adducts (27, 87, 88). A simple mechanism involving only the hexa- to penta-coordination of the heme-Fe atom step preceding the *Av*GReg hemoprotein carbonylation process does not fit the experimental data (data not shown), because it cannot account for the very slow process, characterized by k_1 and k_{-1} (Fig. 8). However, more complex reaction mechanisms (including both parallel and crossing reactions) depicting CO binding to the *Av*GReg hemoprotein can in principle not be excluded. A very unusual feature is the relatively fast rate constant for CO dissociation (*i.e.* $k_{offCO} = 4\ s^{-1}$, Table 1), which is 10–100-fold faster than in both mammalian hemoproteins and those from unicellular species (45). This result suggests that the fast CO dissociation rate constant for *Av*GReg178 is likely related to the electronic distribution of the heme and/or to a stereochemical distortion of the Fe-His proximal bond in the CO-bound form, which have been proposed to play an important role in the CO dissociation rate constant (89, 90). On the other hand, the closely similar CO association rate constant for the bimolecular

process between *Av*GReg178 and mammalian Mbs (Table 1) indeed indicates that the heme pocket of the globin domain is closely related to that of Mb. Because of the assumption made to calculate the multiphasic rate constants, we cannot make any conclusions about the influence of the second domain on the binding kinetics of the globin domain. However, additional domain(s) seem(s) to affect the energy barriers of the ligand pathway approaching the heme pocket, as supported by the complex and multiphasic behavior of the full-length protein (Fig. 8 and Table 1).

The complexity in *Av*GReg178 and *Av*GReg reactivity arises also from biphasic kinetics of hemoprotein deoxygenation. However, in this case it is important to point out that the two phases, present in both *Av*GReg178 and *Av*GReg O_2 dissociation kinetics, seem to refer to two conformations present in the oxygenated form and in slow equilibrium (at least with respect to the observed time regime), such that the relaxation rate of the conformational change $\tau \leq 0.1\ s^{-1}$. The simple O_2 binding equilibrium for *Av*GReg178 and *Av*GReg oxygenation (Fig. 10) implies that the functional difference between the two slow and fast species resides in both association and dissociation rate constants, reflecting two modes of interaction between the bound O_2 and the surrounding protein matrix. In this respect, the fast open conformation appears characterized by a very low activation free energy for the access of the ligand O_2 to the heme pocket for both *Av*GReg178 and *Av*GReg, being characterized by very fast association rate constants (Table 1). The bound O_2 is likely interacting with the distal His(E7), displaying dissociation kinetics closely similar to that observed for mammalian Mbs. On the other hand, the "slow closed" conformation, which shows ligand pathway energetics similar to that displayed by mammalian Mbs, is characterized by comparable values for the association rate constants (Table 1). This conformation shows a very slow O_2 dissociation process, which probably reflects a different interaction of the bound O_2 with distal residues.

As already described under "Results," values of k_{offNO} for NO dissociation from heme-NO-proteins span over 3 orders of magnitude, reflecting structurally different stabilization mode(s) of the heme-bound NO by heme distal residue(s). The stabilization of the heme-bound ligand is achieved mainly by hydrogen bonding to the heme distal His(E7) residue in human Hb, sperm whale, and horse heart Mb, human and mouse Ngb, *G. max* legHb, *E. coli* flavohemoglobin (flavoHb), and possibly in rabbit hemopexin-heme (63, 64, 76, 91–99). In contrast, a hydrogen bonding network involving heme distal Tyr residue(s) stabilizes the heme-bound ligand in human soluble guanylyl cyclase and mycobacterial trHbs (*e.g. M. leprae* trHbO) (66, 100–102). One of these mechanisms of H-bonding can also be postulated for *Av*GReg(178). As indicated in Fig. 1*A*, this can be achieved by involving Tyr(B10).

In addition, values of the second-order rate constant for NO-mediated oxidation of ferrous oxygenated hemeproteins (*i.e.* h_{on}) span also over 3 orders of magnitude (Table 2), reflecting, among others, the accessibility of NO to the heme-O_2 active center, the redox properties of the heme-O_2 adduct, the concomitant presence of two (or more) reacting molecules at the heme site, and values of the rate(s) constants for the formation and the conversion of the reaction intermediate(s) (*e.g.* peroxynitrite) and products (*e.g.* NO_3^-) (35, 74–81). The value of $h_{on}{}^+$ for NO-mediated oxidation of *Av*GReg$^+$-O_2 and *Av*GReg178$^+$-O_2 is favorable when compared with those of related hemeproteins (Table 2), making the NO detoxification role of *Av*GReg$^+$-O_2 and *Av*GReg178$^+$-O_2 likely. Besides the role of ligand sensing, these *in vitro* results may suggest an additional role for *Av*GReg and *Av*GReg178 in NO scavenging. Moreover, values of $k^+{}_{offNO}/k^\#{}_{offNO}$ for *Av*GReg-NO and *Av*GReg178-NO denitrosylation (= 14.0 and 68.0, respectively) and of $h^+{}_{on}/h^\#{}_{on}$ for NO-mediated oxidation of *Av*GReg-O_2 and *Av*GReg178-O_2 (= 12.8 and 63.9, respectively) are similar to those of $k^+{}_{onO2}/k^\#{}_{onO2}$ and $k^+{}_{offO2}/k^\#{}_{offO2}$ for oxygenation and deoxygenation of *Av*GReg-O_2 and *Av*GReg178-O_2 (=14.5 and 79.2, respectively), suggesting that energetically equivalent factors stabilize the open fast and the closed slow *Av*GReg and *Av*GReg178 conformations, in the absence and presence of ligands. The different ligand binding reactions of the heme group are summarized in supplemental data S5.

Acknowledgments—We thank Prof. Giovanni Antonini, Prof. Alberto Boffi, and Dr. Chiara Ciaccio (Rome, Italy) for helpful discussions. We also thank Kirsten Mees and Marie-Louise Van Hauwaert (Antwerp, Belgium) for help with the expression/purification of the recombinant proteins and Anny Bang (Aarhus, Denmark) for technical assistance in the measurement of oxygen equilibria.

REFERENCES

1. Rodgers, K. R. (1999) *Curr. Opin. Chem. Biol.* **3,** 158–167
2. Chan, M. K. (2001) *Curr. Opin. Chem. Biol.* **5,** 216–222
3. Spiro, T. G., and Jarzecki, A. A. (2001) *Curr. Opin. Chem. Biol.* **5,** 715–723
4. Jain, R., and Chan, M. K. (2003) *J. Biol. Inorg. Chem.* **8,** 1–11
5. Sawai, H., Kawada, N., Yoshizato, K., Nakajima, H., Aono, S., and Shiro, Y. (2003) *Biochemistry* **42,** 5133–5142
6. Freitas, T. A., Saito, J. A., Hou, S., and Alam, M. (2005) *J. Inorg. Biochem.* **99,** 23–33
7. Gilles-Gonzalez, M. A., and Gonzalez, G. (2005) *J. Inorg. Biochem.* **99,** 1–22
8. Rodgers, K. R., and Lukat-Rodgers, G. S. (2005) *J. Inorg. Biochem.* **99,** 963–977
9. Schmidt, A. J., Ryjenkov, D. A., and Gomelsky, M. (2005) *J. Bacteriol.* **187,** 4774–4781
10. Chang, A. L., Tuckerman, J. R., Gonzalez, G., Mayer, R., Weinhouse, H., Volman, G., Amikam, D., Benziman, M., and Gilles-Gonzalez, M. A. (2001) *Biochemistry* **40,** 3420–3426
11. Roberts, G. P., Kerby, R. L., Youn, H., and Conrad, M. (2005) *J. Inorg. Biochem.* **99,** 280–292
12. Hou, S., Larsen, R. W., Boudko, D., Riley, C. W., Karatan, E., Zimmer, M., Ordal, G. W., and Alam, M. (2000) *Nature* **403,** 540–544
13. Sousa, E. H., Gonzalez, G., and Gilles-Gonzalez, M. A. (2005) *Biochemistry* **44,** 15359–15365
14. Tal, R., Wong, H. C., Calhoon, R., Gelfand, D., Fear, A. L., Volman, G., Mayer, R., Ross, P., Amikam, D., Weinhouse, H., Cohen, A., Sapir, S., Ohana, P., and Benziman, M. (1998) *J. Bacteriol.* **180,** 4416–4425
15. Amikam, D., and Benziman, M. (1989) *J. Bacteriol.* **171,** 6649–6655
16. Ross, P., Mayer, R., and Benziman, M. (1991) *Microbiol. Rev.* **55,** 35–58
17. Zhang, W., Olson, J. S., and Phillips, G. N., Jr. (2005) *Biophys. J.* **88,** 2801–2814
18. Yoshimura, H., Yoshioka, S., Kobayashi, K., Ohta, T., Uchida, T., Kubo, M., Kitagawa, T., and Aono, S. (2006) *Biochemistry* **45,** 8301–8307
19. Freitas, T. A., Hou, S., and Alam, M. (2003) *FEBS Lett.* **552,** 99–104
20. Conrad, R. (1996) *Microbiol. Rev.* **60,** 609–640
21. Youn, H., Kerby, R. L., Conrad, M., and Roberts, G. P. (2004) *J. Bacteriol.* **186,** 1320–1329

22. Ye, R. W., Averill, B. A., and Tiedje, J. M. (1994) *Appl. Environ. Microbiol.* **60,** 1053–1058
23. Galperin, M. Y., Nikolskaya, A. N., and Koonin, E. V. (2001) *FEMS Microbiol. Lett.* **203,** 11–21
24. Ryjenkov, D. A., Tarutina, M., Moskvin, O. V., and Gomelsky, M. (2005) *J. Bacteriol.* **187,** 1792–1798
25. Simm, R., Morr, M., Kader, A., Nimtz, M., and Romling, U. (2004) *Mol. Microbiol.* **53,** 1123–1134
26. Romling, U. (2005) *Cell. Mol. Life Sci.* **62,** 1234–1246
27. Dewilde, S., Kiger, L., Burmester, T., Hankeln, T., Baudin-Creuza, V., Aerts, T., Marden, M. C., Caubergs, R., and Moens, L. (2001) *J. Biol. Chem.* **276,** 38949–38955
28. Geuens, E., Brouns, I., Flamez, D., Dewilde, S., Timmermans, J. P., and Moens, L. (2003) *J. Biol. Chem.* **278,** 30417–30420
29. Wright, E., and Serpersu, E. H. (2004) *Protein Expression Purif.* **35,** 373–380
30. Stoll, S., and Schweiger, A. (2006) *J. Magn. Reson.* **178,** 42–55
31. Antonini, E., and Brunori, M. (1971) *Biochim. Biophys. Acta* **310,** 309–316
32. Hayashi, A., Suzuki, T., and Shin, M. (1973) *Biochim. Biophys. Acta* **310,** 309–316
33. Fago, A., Hundahl, C., Dewilde, S., Gilany, K., Moens, L., and Weber, R. E. (2004) *J. Biol. Chem.* **279,** 44417–44426
34. Weber, R. E. (1992) *J. Appl. Physiol.* **72,** 1611–1615
35. Ascenzi, P., and Visca, P. (2008) *Methods Enzymol.*, in press
36. Hoshino, M., Maeda, M., Konishi, R., Seki, H., and Ford, P. C. (1996) *J. Am. Chem. Soc.* **118,** 5702–5707
37. Moore, E. G., and Gibson, Q. H. (1976) *J. Biol. Chem.* **251,** 2788–2794
38. Mendes, P. (1993) *Comput. Appl. Biosci.* **9,** 563–571
39. Mendes, P. (1997) *Trends Biochem. Sci.* **22,** 361–363
40. Mendes, P., and Kell, D. (1998) *Bioinformatics* (*Oxf.*) **14,** 869–883
41. Trent, J. T., III, Hvitved, A. N., and Hargrove, M. S. (2001) *Biochemistry* **40,** 6155–6163
42. Vinogradov, S. N., Hoogewijs, D., Bailly, X., Arredondo-Peter, R., Guertin, M., Gough, J., Dewilde, S., Moens, L., and Vanfleteren, J. R. (2005) *Proc. Natl. Acad. Sci. U. S. A.* **102,** 11385–11389
43. Edgar, R. C. (2004) *BMC Bioinformatics* **5,** 113
44. Nicholas, K. B., Nicholas, H. B., Jr., and Deerfield, D. W., II (1997) *EMBNET. News* **4,** 1–4
45. Das, T. K., Weber, R. E., Dewilde, S., Wittenberg, J. B., Wittenberg, B. A., Yamauchi, K., Van Hauwaert, M. L., Moens, L., and Rousseau, D. L. (2000) *Biochemistry* **39,** 14330–14340
46. Arredondo-Peter, R., Hargrove, M. S., Sarath, G., Moran, J. F., Lohrman, J., Olson, J. S., and Klucas, R. V. (1997) *Plant Physiol.* **115,** 1259–1266
47. Duff, S. M., Wittenberg, J. B., and Hill, R. D. (1997) *J. Biol. Chem.* **272,** 16746–16752
48. Hu, S., Smith, K. M., and Spiro, T. G. (1996) *J. Am. Chem. Soc.* **118,** 12638–12646
49. Aono, S., Kato, T., Matsuki, M., Nakajima, H., Ohta, T., Uchida, T., and Kitagawa, T. (2002) *J. Biol. Chem.* **277,** 13528–13538
50. Uchida, T., and Kitagawa, T. (2005) *Acc. Chem. Res.* **38,** 662–670
51. Peterson, E. S., Friedman, J. M., Chien, E. Y., and Sligar, S. G. (1998) *Biochemistry* **37,** 12301–12319
52. Taylor, C. P. (1977) *Biochim. Biophys. Acta* **491,** 137–148
53. Svistunenko, D. A., Sharpe, M. A., Nicholls, P., Blenkinsop, C., Davies, N. A., Dunne, J., Wilson, M. T., and Cooper, C. E. (2000) *Biochem. J.* **351,** 595–605
54. Blumberg, W. E., and Peisach, J. (1971) in *Probes of Structure and Function of Macromolecules and Membranes* (Chance, B., Yonetani, T., and Mildvan, A. S., eds) p. 215, Academic Press, New York
55. Peisach, J., Blumberg, W. E., Lode, E. T., and Coon, M. J. (1971) *J. Biol. Chem.* **246,** 5877–5881
56. Walker, F. A., Scheidt, W. R., and Osvarth, S. R. (1986) *J. Am. Soc. Trans.* **108,** 5288–5297
57. Quinn, R., Valentine, J. S., Byrn, M. P., and Strouse, C. E. (1987) *J. Am. Chem. Soc.* **109,** 3301–3308
58. Das, T. K., Couture, M., Lee, H. C., Peisach, J., Rousseau, D. L., Wittenberg, B. A., Wittenberg, J. B., and Guertin, M. (1999) *Biochemistry* **38,** 15360–15368
59. Ascenzi, P., Bolognesi, M., and Visca, P. (2007) *Biochem. Biophys. Res. Commun.* **357,** 809–814
60. Fasano, M., Antonini, G., and Ascenzi, P. (2006) *Biochem. Biophys. Res. Commun.* **345,** 704–712
61. Herold, S., and Rock, G. (2005) *Biochemistry* **44,** 6223–6231
62. Van Doorslaer, S., Dewilde, S., Kiger, L., Nistor, S. V., Goovaerts, E., Marden, M. C., and Moens, L. (2003) *J. Biol. Chem.* **278,** 4919–4925
63. Brucker, E. A., Olson, J. S., Ikeda-Saito, M., and Phillips, G. N., Jr. (1998) *Proteins* **30,** 352–356
64. Hargrove, M. S., Barry, J. K., Brucker, E. A., Berry, M. B., Phillips, G. N., Jr., Olson, J. S., Arredondo-Peter, R., Dean, J. M., Klucas, R. V., and Sarath, G. (1997) *J. Mol. Biol.* **266,** 1032–1042
65. Kharitonov, V. G., Sharma, V. S., Magde, D., and Koesling, D. (1997) *Biochemistry* **36,** 6814–6818
66. Martin, E., Berka, V., Bogatenkova, E., Murad, F., and Tsai, A. L. (2006) *J. Biol. Chem.* **281,** 27836–27845
67. Gow, A. J., Luchsinger, B. P., Pawloski, J. R., Singel, D. J., and Stamler, J. S. (1999) *Proc. Natl. Acad. Sci. U. S. A.* **96,** 9027–9032
68. Brunori, M. (2001) *Trends Biochem. Sci.* **26,** 209–210
69. Flogel, U., Merx, M. W., Godecke, A., Decking, U. K., and Schrader, J. (2001) *Proc. Natl. Acad. Sci. U. S. A.* **98,** 735–740
70. Frauenfelder, H., McMahon, B. H., and Fenimore, P. W. (2003) *Proc. Natl. Acad. Sci. U. S. A.* **100,** 8615–8617
71. Brunori, M., Bourgeois, D., and Vallone, B. (2004) *J. Struct. Biol.* **147,** 223–234
72. Frey, A. D., and Kallio, P. T. (2005) *Trends Biotechnol.* **23,** 69–73
73. Poole, R. K. (2005) *Biochem. Soc. Trans.* **33,** 176–180
74. Gardner, P. R., Gardner, A. M., Brashear, W. T., Suzuki, T., Hvitved, A. N., Setchell, K. D., and Olson, J. S. (2006) *J. Inorg. Biochem.* **100,** 542–550
75. Brunori, M., Giuffrè, A., Nienhaus, K., Nienhaus, G. U., Scandurra, F. M., and Vallone, B. (2005) *Proc. Natl. Acad. Sci. U. S. A.* **102,** 8483–8488
76. Gardner, A. M., Martin, L. A., Gardner, P. R., Dou, Y., and Olson, J. S. (2000) *J. Biol. Chem.* **275,** 12581–12589
77. Herold, S., Exner, M., and Nauser, T. (2001) *Biochemistry* **40,** 3385–3395
78. Herold, S., and Puppo, A. (2005) *J. Biol. Inorg. Chem.* **10,** 935–945
79. Ouellet, H., Ouellet, Y., Richard, C., Labarre, M., Wittenberg, B., Wittenberg, J., and Guertin, M. (2002) *Proc. Natl. Acad. Sci. U. S. A.* **99,** 5902–5907
80. Ouellet, H., Juszczak, L., Dantsker, D., Samuni, U., Ouellet, Y. H., Savard, P. Y., Wittenberg, J. B., Wittenberg, B. A., Friedman, J. M., and Guertin, M. (2003) *Biochemistry* **42,** 5764–5774
81. Ascenzi, P., Bocedi, A., Bolognesi, M., Fabozzi, G., Milani, M., and Visca, P. (2006) *Biochem. Biophys. Res. Commun.* **339,** 450–456
82. Hecht, G. B., Lane, T., Ohta, N., Sommer, J. M., and Newton, A. (1995) *EMBO J.* **14,** 3915–3924
83. Uzan, J., Dewilde, S., Burmester, T., Hankeln, T., Moens, L., Hamdane, D., Marden, M. C., and Kiger, L. (2004) *Biophys. J.* **87,** 1196–1204
84. Sawai, H., Makino, M., Mizutani, Y., Ohta, T., Sugimoto, H., Uno, T., Kawada, N., Yoshizato, K., Kitagawa, T., and Shiro, Y. (2005) *Biochemistry* **44,** 13257–13265
85. Sage, J. T., Morikis, D., and Champion, P. M. (1991) *Biochemistry* **30,** 1227–1237
86. Springer, B. A., Sligar, S. G., Olson, J. S., and Phillips, G. N. J. (1994) *Chem. Rev.* **94,** 699–714
87. de Sanctis, D., Pesce, A., Nardini, M., Bolognesi, M., Bocedi, A., and Ascenzi, P. (2004) *IUBMB Life* **56,** 643–651
88. Smagghe, B. J., Sarath, G., Ross, E., Hilbert, J. L., and Hargrove, M. S. (2006) *Biochemistry* **45,** 561–570
89. White, D. K., Cannon, J. B., and Traylor, T. G. (1979) *J. Am. Chem. Soc.* **101,** 2443–2454
90. Brunori, M., Ascenzi, P., and Coletta, M. (1986) in *Supermolecules: Biological and Chemical Aspects* (Montanari, U., ed) pp. 55–73, Atti Accademia Nazionale dei Lincei, Rome
91. Chan, N. L., Rogers, P. H., and Arnone, A. (1998) *Biochemistry* **37,** 16459–16464

92. Paoli, M., Anderson, B. F., Baker, H. M., Morgan, W. T., Smith, A., and Baker, E. N. (1999) *Nat. Struct. Biol.* **6,** 926–931
93. Ilari, A., Bonamore, A., Farina, A., Johnson, K. A., and Boffi, A. (2002) *J. Biol. Chem.* **277,** 23725–23732
94. Copeland, D. M., West, A. H., and Richter-Addo, G. B. (2003) *Proteins* **53,** 182–192
95. de Sanctis, D., Pesce, A., Nardini, M., Bolognesi, M., Bocedi, A., and Ascenzi, P. (2004) *IUBMB Life* **56,** 643–654
96. Pesce, A., Dewilde, S., Nardini, M., Moens, L., Ascenzi, P., Hankeln, T., Burmester, T., and Bolognesi, M. (2003) *Structure* (*Camb.*) **11,** 1087–1095
97. Vallone, B., Nienhaus, K., Brunori, M., and Nienhaus, G. U. (2004) *Proteins* **56,** 85–92
98. Vallone, B., Nienhaus, K., Matthes, A., Brunori, M., and Nienhaus, G. U. (2004) *Proc. Natl. Acad. Sci. U. S. A.* **101,** 17351–17356
99. Ascenzi, P., Bellelli, A., Coletta, M., Colosimo, A., Falcioni, G., Giacometti, G. M., Ippoliti, R., Zolla, L., and Giardina, B. (2007) *IUBMB Life* **59,** 600–619
100. Milani, M., Savard, P. Y., Ouellet, H., Ascenzi, P., Guertin, M., and Bolognesi, M. (2003) *Proc. Natl. Acad. Sci. U. S. A.* **100,** 5766–5771
101. Milani, M., Pesce, A., Nardini, M., Ouellet, H., Ouellet, Y., Dewilde, S., Bocedi, A., Ascenzi, P., Guertin, M., Moens, L., Friedman, J. M., Wittenberg, J. B., and Bolognesi, M. (2005) *J. Inorg. Biochem.* **99,** 97–109
102. Visca, P., Fabozzi, G., Petrucca, A., Ciaccio, C., Coletta, M., De Sanctis, G., Bolognesi, M., Milani, M., and Ascenzi, P. (2002) *Biochem. Biophys. Res. Commun.* **294,** 1064–1070
103. Brunori, M., and Schuster, T. M. (1969) *J. Biol. Chem.* **244,** 4046–4053
104. Gibson, Q. H., Olson, J. S., McKinnie, R. E., and Rohlfs, R. J. (1986) *J. Biol. Chem.* **261,** 10228–10239
105. Zhang, W., and Phillips, G. N., Jr. (2003) *Structure* (*Camb.*) **11,** 1097–1110